MODELING INFLOWS INTO STRATIFIED LAKES WITH VERTICAL SCALE DISTORTION

By

GENE EDWARD KOUBA

Bachelor of Science

Oklahoma State University

Stillwater, Oklahoma

1972

Submitted to the Faculty of the Graduate College
of the Oklahoma State University
in partial fulfillment of the requirements
for the Degree of
MASTER OF SCIENCE
July, 1974

MODELING INFLOWS INTO STRATIFIED LAKES WITH

VERTICAL SCALE DISTORTION

Thesis Approved:

Dennis K McLaughlin
Thesis Adviser

W. A. Tiedeman

Robert M. Morris

N. N. Durham
Dean of the Graduate College

ACKNOWLEDGEMENTS

There are numerous persons who have given much of their time and effort in helping me with this research. The following deserve more thanks than they will probably ever receive:

My major advisor, Dr. Dennis K. McLaughlin, and committee members Dr. Peter Moretti and Dr. William Tiederman for their guidance and assistance throughout my graduate program.

My good friends, Mike Karpuk, Trouser Troutt, Nadar Sharabianlou, Tom Gibson, Willie Adcox, Roger Elliot and others for research assistance, counseling, and therapeutic "Bull" sessions.

My family for moral and financial support whenever needed.

This research project was supported by the Oklahoma Water Resources Research Institute.

TABLE OF CONTENTS

LIST OF TABLES

LIST OF FIGURES

Figure Page

NOMENCLATURE

D	width of diffusion layer
Fr	Froude number, $\frac{U}{(gH)^{\frac{1}{2}}}$
g	gravitational constant
H	depth of lake
J	Richardson number, $g \frac{\partial\rho/\partial z}{\rho_c(\partial u/\partial z)^2}$
$\overline{J}$	overall average Richardson number, $\frac{g\Delta\rho L_2^2}{\rho_c U_c^2 L_1}$
L	characteristic length or a subscript to denote large or deep model
L_1	characteristic length
L_2	characteristic length
ℓ	length of lake
Q_i	flowrate of inflow into lake
Re	Reynolds number, $\frac{U_c L}{\nu}$
S	subscript to denote small or shallow lake model
t	time after inflow reaches inlet
U_c	characteristic velocity
V_i	inflow velocity at inlet
x	downstream horizontal dimension
z	vertical dimension

GREEK LETTERS

Δ - difference

υ - dynamic viscosity of the fluid

ν - kinematic viscosity of the fluid

ρ - density of the fluid

ρ_c - characteristic density

ρ_i - density of the inflowing fluid

ρ_2 - density of lighter upper fluid in stratified lake

ρ_3 - density of heavier bottom fluid in stratified lake

ρ^* - non-dimensional density, $\frac{\rho - \rho_2}{\rho_3 - \rho_2}$

CHAPTER I

INTRODUCTION

The problems associated with the distribution of fluid inflow into stratified lakes are of ever increasing importance among those concerned with lake ecology. Consider a stratified lake consisting of three main regions: a top layer of the lightest fluid, a bottom layer of the densest fluid and a mid-region increasing in density with depth. This is a natural situation which can occur with the changing of the seasons and which is enhanced by the dissolving of minerals in the water.

Fluid inflows may introduce a wide variety of additional problems into the lake. Power plants for instance, discharge large quantities of thermal energy into lakes and reservoirs. Rivers and creeks carry farm and feed lot run-off plus the extra burden of industrial pollution into the lakes. Different combinations of these situations may produce a wide range of complex effects on the lake ecology. Some of these effects may be beneficial and others may be undesirable, but in most cases the long range results are unknown and seemingly unpredictable. The distribution of inflows into stratified lakes and the resulting lake ecology can be studied on a particular lake but detailed studies of this sort require large amounts of time, effort and money. This type investigation lacks versatility plus there is the possibility of ruining the lake in the process.

Therefore it is desirable and necessary to be able to model fluid inflows into stratified lakes. Studies on expected changes in inflow rates, thermal load, silt load, pollution level, etc., can be made on a model with the expected result of predicting distribution of heat, silt, and pollutants due to the interaction of the inflow with the lake. In many cases this might be done prior to the actual inflow and lake conditions being studied. Modeling could give basic information necessary to predict the effects of thermal discharges, addition of pollutants or large silt loads in terms of distribution. Therefore biological activity might be predicted since the distribution of heat, pollutants and minerals will largely determine the biological activity.

There are a number of problems associated with any type of hydraulic modeling study. For instance in designing a scale model of a lake, special care must be given to the size of the model so that viscous forces do not become over-emphasized. (Viscous forces become more prominent as the size and depth of the model is decreased.) One solution is to build a large and cumbersome model, but this has one extreme disadvantage - cost. Also a model of this type is impractical for modeling very large lakes. By exaggerating the vertical side, a smaller and consequently cheaper laboratory size model can be built without allowing the viscous forces to predominate in the model and destroying the dynamic similarity between the model and the real lake system. By sacrificing some portion of geometric similarity and exaggerating the vertical scale, the total size of the model can be reduced and the similarity between the roles of the dominating forces is preserved.

In many modeling problems similarity trade-offs of this type are very important since the original system being modeled is often a

unique one. In this compromise between geometric and dynamic similarity, it is the question of relative importance placed on the interaction of the various pairs of forces that has produced a lack of universal acceptance of vertical scale distortion. Consequently there exists considerable disagreement among researchers about the validity and worthiness of distorting the vertical scale. Fischer and Holly (5) are doubtful of the usefulness of the concept applied to models in studies of pollutant dispersion. They maintain that the result of exaggerating the vertical scale is to magnify the dispersive effects of vertical velocity gradients and diminish the effects of transverse gradients. On the other hand, the utilization of scale exaggeration was reported in Keulegan's (9) studies and also by Barr (1) as being a workable concept as long as the effects of scale exaggeration were taken into account.

Although an exact similarity between model and real lake system is unlikely, some degree of similarity is possible and with knowledge of the effects of vertical scale distortion this concept can be a useful modeling tool when properly applied. The development of some insight into the problems, limitations, and applications of the concept of vertical scale exaggeration is the primary concern of this experimental study.

Problem Statement

The purpose of this experimental study was to evaluate the effect of vertical scale exaggeration in modeling fluid inflows into stratified lakes. In order to do this the effects of an enlarged vertical

scale were isolated by using two plexiglass models identical in the horizontal dimensions and scaled 2:1 vertically.

Figure 1 is a sketch of the specific physical situation that was modeled. It consists of a lake stratified into two distinct layers of water separated by a region varying in density from the lighter upper layer to the heavier lower layer. The effects of vertical scale distortion were studied by first arranging a specific initial stratification in the prototype model, establishing an intermediate density inflow into the lake and visually recording the flow patterns. Then the appropriate initial stratifications and inflows were arranged in the deeper, distorted model in order to simulate the flow patterns of the prototype model. Comparisons of inflow patterns and distributions were made to examine critical flow parameters to determine their effect on proper simulation between the models and to gain insight on the consequence of distorting the vertical scale. To properly model a specified flow configuration, it was necessary to develop a modeling criteria that would adjust various control variables of the distorted model to yield flow situations respectively similar to those of the prototype model.

CHAPTER II

MODELING TECHNIQUE

In examining the physical situation that was modeled (see Figure 1) it can be seen that the main flow variables are inlet velocity, density difference, and diffusion layer thickness. These flow variables combined with the fluid properties and the geometry of the system can be used to form three non-dimensional parameters. Listed below are these three parameters important in the modeling of free-surface stratified hydraulic systems.

1. Froude Number

$$Fr = \frac{U}{(gH)^{\frac{1}{2}}}$$

2. Reynolds Number

$$Re = \frac{\rho U_c L}{\mu}$$

3. Richardson Number

$$J = \frac{-g\ \partial\rho/\partial z}{\rho_c (\partial u/\partial z)^2}$$

In order to limit the scope of this investigation, only inflows with velocities much less than the surface wave velocity $(gH)^{\frac{1}{2}}$ are considered. The surface wave phenomenon is then negligible and the Froude Number need not be considered.

In general for turbulent flow situations when the Reynolds number is sufficiently large, the fluid dynamics are not critically sensitive to change in Reynolds number. Ellison and Turner (4) found that the turbulent entrainment in stratified flows is a function only of the Richardson number provided the Reynolds number is sufficiently large and the density differences are small. But here questions arise concerning the proper definition and appropriate size of the Reynolds number in relation to expected density differences. Using the flow variables, the Reynolds number was expressed as $Re = \frac{V_i D}{\nu}$, where V_i is the inlet velocity and D is the diffusion layer thickness. The kinematic viscosity, ν does not change appreciably over small density changes and is assumed constant. Since the magnitude of this Reynolds number was not expected to be so large that the flow was entirely Richardson number dependent, it was necessary to consider the Reynolds number dependence.

However, the stability and the decaying of turbulence in stratified flow situations are usually associated with the Richardson number. Therefore it is expected that the Richardson number is the more important parameter and that the flow is somewhat less dependent upon the Reynolds number. For modeling purposes an overall average Richardson number can be formed by assuming that the density gradient, $\partial\rho/\partial z$ scales with $\Delta\rho/L_1$ where $\Delta\rho$ is the density difference between two layers of fluid, and that the velocity gradient, $\partial u/\partial z$, scales with $\frac{U_c}{L_2}$ where U_c represents a characteristic velocity. L_1 and L_2 are characteristic lengths. The overall Richardson number is then $\overline{J} = \frac{g\Delta\rho L_2^2}{\rho_c U_c^2 L_1}$, where the bar indicates an overall average. Since the vertical scale of one

model is exaggerated, the choice between horizontal and vertical length scales or a combination of both to represent the characteristic lengths L_1 and L_2 complicates the problem of defining an overall Richardson number. Either scale could be used if scale distortion were not employed. But when the vertical scale factor differs from the horizontal scale factor, different combinations of length scales will yield different $\overline{J}$ values.

In scaling the density gradient $\partial\rho/\partial z$ with $\Delta\rho/L_1$, two characteristic depths seem appropriate for L_1: the depth of the lake (H) and the thickness of the diffusion layer (D) between the light fluid on top and the denser fluid on bottom. There appears to be no justification for selecting a horizontal length scale for the vertical density gradient. In the case of the velocity gradient $\frac{\partial U}{\partial z}$ there are three possible length scales for L_2. They are: (1) the depth of the lake (H), (2) the length of the lake (ℓ) and (3) the thickness of the diffusion layer (D). Thus $\Delta\rho/L_1$ may assume two forms, $\Delta\rho/H$ and $\Delta\rho/D_1$ and U_c/L_2 may assume three forms, U_c/H, U_c/ℓ, U_c/D. This results in six different possibilities of expressing an overall Richardson number. Each of these will be referred to as an overall Richardson number $\overline{J}_i$ where "i" represents the appropriate subscript indicating a particular non-dimensional grouping. The inlet velocity, V_i was chosen as the characteristic velocity in the velocity gradient. The non-dimensional groupings are described below for each of the six cases.

Case 1: $\partial\rho/\partial z \sim \Delta\rho/H$ and $\partial u/\partial z \sim V_i/\ell$

$$\overline{J}_1 = \frac{g\Delta\rho\ell^2}{\rho_c V_i^2 H}$$

Case 2: $\partial\rho/\partial z \sim \Delta\rho/H$ and $\partial u/\partial z \sim V_i/H$

$$\bar{J}_2 = \frac{g\Delta\rho H}{\rho_c V_i^2}$$

Case 3: $\partial\rho/\partial z \sim \Delta\rho/D$ and $\partial u/\partial z \sim V_i/\ell$

$$\bar{J}_3 = \frac{g\Delta\rho \ell^2}{\rho_c V_i^2 D}$$

Case 4: $\partial\rho/\partial z \sim \Delta\rho/D$ and $\partial u/\partial z \sim V_i/D$

$$\bar{J}_4 = \frac{g\Delta\rho D}{\rho_c V_i^2}$$

Case 5: $\partial\rho/\partial z \sim \Delta\rho/H$ and $\partial u/\partial z \sim V_i/D$

$$\bar{J}_5 = \frac{g\Delta\rho D^2}{\rho_c V_i^2 H}$$

Case 6: $\partial\rho/\partial z \sim \Delta\rho/D$ and $\partial u/\partial z \sim V_i/H$

$$\bar{J}_6 = \frac{g\Delta\rho H^2}{\rho_c V_i^2 D}$$

There are three variables $\Delta\rho/\rho_c$, V_i and D which can be controlled to produce different values for each of the $\bar{J}_i$'s. ρ_c is a characteristic density in this case the density of the heaviest bottom fluid is used. If D, the diffusion thickness, is scaled with the vertical scale factor, this will limit the number of groupings to two basic non-dimensional Richardson parameters. The key difference is in the relationship between $\Delta\rho/\rho_c$ and V_i between the two models. For instance in using either $\bar{J}_1$ or $\bar{J}_3$ as the modeling parameter for matching the deep (exaggerated) model to the shallow model, the relationship between the

control variables is $\left(\frac{\Delta\rho}{\rho_c V_i^2}\right)_L = 2\left(\frac{\Delta\rho}{\rho_c V_i^2}\right)_S$. The subscripts L and S denote the large deep lake model and the shallow lake model respectively. For any of the other non-dimensional groupings, the control variables are related by $\left(\frac{\Delta\rho}{\rho_c V_i^2}\right)_L = \frac{1}{2}\left(\frac{\Delta\rho}{\rho_c V_i^2}\right)_S$. The pronounced difference between the two relationships of the control variables will produce radically differing flow configurations on the two lakes for comparison. This basic difference stems from the scaling of the velocity gradient with a horizontal length in $\bar{J}_1$ and $\bar{J}_3$ and a vertical height in the rest. Even though absolute control in scaling D was not possible making it necessary to consider all six parameters, the basic difference in the grouping still remained very pronounced.

A matrix was formed in which each non-dimensional $\bar{J}$ for various flow configurations on one lake model could be compared to matching $\bar{J}$'s of different flow configuration on the other model. In this way one specific flow situation on the large model may match several different non-dimensional groupings corresponding to various flow situations on the small lake model and vice versa. Flow visualizations and density profile measurements were to indicate which matchings of the non-dimensional groupings yielded the best flow simulation between the two models.

All of the non-dimensional groupings are based on the initial stratification and the inlet velocity, but as the inflow penetrates into the lake, the density gradient decreases, the behavior of the velocity gradient is unknown and consequently the local Richardson number $\frac{g\ \partial\rho/\partial z}{\rho_c(\partial u/\partial z)^2}$ changes in some unknown manner. This is yet another

aspect of the modeling problem which cannot be critically examined in this experimental investigation.

CHAPTER III

EXPERIMENTAL ARRANGEMENT

In this chapter the experimental apparatus and procedures are described. The test facilities are essentially those used by S. J. Vogel (15) with some additions and modifications.

Lake Models and Inflow System

Figure 2 is a sketch of the experimental facility consisting of storage tanks, flow lines, flow meter and lake model. Two lake models are used for determining the effect of scale distortion. Both lakes are eight feet long and 18 inches wide and made of 1/2 inch plexiglass to allow observation of flow into and through the lakes. The models are 12 and six inches high and filled to depths of four and two inches yielding a vertical scale factor of two.

The inlets to the lakes are constructed of 1/2 inch plexiglass and are one inch wide inside. Connected to the inlet and inside the lakes are fiberglass formed contours. The top view of Figure 1 shows equi-depth lines for the contours. Like the lake models the contours are identical in horizontal dimensions and distorted 2:1 in the vertical dimensions.

A schematic diagram of the inflow and dye injection systems is shown in Figure 3. The various salt solutions are prepared in two elevated 45 gallon plastic storage tanks situated on the upper deck of

the laboratory. Each solution can be gravity fed into the lake. From the flow-meter the inflow is introduced into the inlet channel entrance pipe, then passes through a screen and into the one inch wide portion of the inlet. As the inflow enters the lake it flows down the channeled contour and deeper into the lake.

Square weir attachments at the opposite ends of the lakes provide the outlet and maintains the lakes at a constant level. A dye injection system is located upstream from the inlet to allow thorough mixing of the dye with the inflow. This system also allowed the inflow to be dyed at any time during the test run. Red and green food coloring served as the dye.

Data Collection Systems

Two different methods were employed to critically examine the accuracy of the modeling technique. The main method used for data collection was a photographic record of the top and side views of the dyed portion of the inflow as it progressed through the test section of the lake. This was accomplished by means of the mirror systems shown in Figure 4. Two mirror systems were utilized, one for the top view and one for the side view of the test section. The test section was a two foot long section of the lake positioned from 27-51 inches downstream from the lake inlet. In this span of the lake, the inflow lifted off the contour and began to lens between the two layers of fluid.

A 35mm camera was positioned on a tripod approximately ten feet from the lake model. A clock was situated beneath the top mirror so that on each photograph the side view, the top view and the time would be recorded. Grid patterns on the lake models aided in the

determination of the location of the dye patterns. By taking a series of photographs at one to three second intervals of the dyed inflow progressing through the test section, the flow pattern for each test are recorded.

The other method was the comparison of initial and final density profiles obtained through the use of a conductivity probe. The resistivity of salt solutions varies with density thereby providing a means for measuring the density profiles. The details of construction and operation of the probe are given in Appendix A.

Experimental Procedure

In this section the testing sequence is outlined with special consideration given to determining the control variables ρ_i, ρ_2, ρ_3, V_i and D. The relationship between these variables depends on the value of the particular non-dimensional grouping being matched.

The testing program evolved from the basic theoretical considerations presented in Chapter II. First one non-dimensional grouping from the six $\overline{J}_i$'s was chosen as the modeling parameter between the two lakes. Then a value was selected for this $\overline{J}_i$ with regard to reasonable configurations of the test variables on either lake. With this preliminary testing design at hand, the actual testing program was begun.

First either lake being tested was filled with tap water and appropriate solutions prepared in the elevated tanks. Allowing the solutions to stand for several hours permitted the dissolved gases to be released as the temperature of the fluids reached room temperature. Since the conductivity probes were calibrated at room temperature, all density measurements were made at room temperature.

Next the heavy fluid (ρ_3) was introduced into the lake providing the initial stratification. Different filling techniques were employed on each model in an effort to produce the desired stratification and diffusion thickness. In general the heavy fluid would mix with the tap water as it filled the lower half of the lake model. How much the heavy fluid was diluted by this mixing depended on the means of filling and the flowrate. The thickness of the diffusion layer was largely controlled by the same two factors. In order to produce a fairly sharp profile on the small model, the heavy fluid was introduced into the lake by means of a 1/4 inch diameter plastic hose. The hose was placed on the bottom of the lake with a shield over it. This reduced the amount of fresh water that the heavy water was exposed to and resulted in a fairly sharp and somewhat controllable interfacial thickness. On the large lake model the heavy fluid was allowed to flow down the contour into the lake at a much higher flowrate than for the filling of the small lake. This resulted in much more mixing which produced a much larger diffusion layer. In this way the diffusion layers could be scaled roughly the same as the vertical scale distortion.

The stratified lake was then allowed to settle for four to eight hours before the initial vertical density profile was taken with the conductivity probe. From this profile an average slope was determined through the nearly linear region of the diffusion layer. The intersection of the slope with the maximum and minimum densities yielded a distance D, the thickness of the interface. Figure 5 shows a typical density profile and slope through the interface. With these control variables set ρ_2, ρ_3, and D, the inlet velocity can be altered to

produce the desired relationship between flow variables according to the modeling parameter used. The density of the inflow was restricted to an intermediate density between ρ_2 and ρ_3 as specified in the Problem Statement. This intermediate density was selected so that the inflow would flow in between the layers near the half-depth of the lake.

Once the intermediate density fluid was prepared in the elevated tank and the lake had settled the required amount of time, the inflow was admitted into the lake. The inflow flowrate was gradually brought up to the predetermined setting and the timer was started as the flow entered the lake. The dye was not injected until the start-up transient time had expired. In this context, the start-up transient time might be considered another important variable. While it is necessary for the transient to pass through the test section before dye is injected into the flow, once the transient passes the flow is assumed to be quasi-steady-state so that the exact time for injection is not critical. Therefore the undyed inflow was allowed to progress through the test section then the dye was injected into the inflow mixing thoroughly before entering the lake. As the dyed portion entered the lake, the timer reading was noted, this time when non-dimensionalized with the flowrate and lake volume provided a time scale for the start-up transient time. Then approximately 20 photographs were taken of the dye front moving through the test section. After the photographs were taken the dye injection was shut off and the inflow allowed to flow for the specified period of time, usually the amount of time for the dyed portion to reach the lake outlet. The inflow was then shut off and the time recorded. The last test measurement was the final vertical density profile of the lake usually taken within ten minutes after the inflow was shut off. The

density profiles were determined from eight equally spaced conductivity probe readings in the middle of either lake.

The independent variables of the test run were:

(1) the initial density profile

(2) the extreme densities of the upper and lower strata

(3) the diffusion thickness

(4) the inflow rate determined from 1, 2, and 3

(5) the inflow density also determined from 1, 2, and 3

And the outputs were:

(6) timed photographs of top and side views

(7) the final density profile

Each test run was set up so that at least one $\overline{J}_i$ would match the corresponding $\overline{J}_i$ for a particular test on the other model. By forming a matrix of these test runs versus the different $\overline{J}_i$'s, several combinations of matching $\overline{J}_i$'s are compared. The number of different combinations formed in this matrix was largely limited by the difficulty in producing actual test configurations of the control variables that exactly matched the preliminary test configurations. But with some planning a test run could usually be set up on one lake model so that at least one of its non-dimensional parameters would match the corresponding $\overline{J}_i$ on one of the test runs on the other model. Appendix B contains the matrix of $\overline{J}_i$'s versus test runs on the lakes.

Data Reduction

The initial and final vertical density profiles were replotted in terms of a normalized non-dimensional density, $\rho^* = \frac{\rho - \rho_2}{\rho_3 - \rho_2}$, versus a non-dimensional height, $\frac{z}{H}$. (Figures 5 and 6) Plots such as these

provided comparisons of the shapes and slopes for the initial and final profiles of corresponding test runs. The initial profiles plotted in Figure 5 showed good agreement in shape and slope. The final profiles in Figure 6 show reasonable agreement in shape and slope but are displaced slightly. The density of the inflow was less relative to the density difference in the lake for the deep lake run than for the shallow lake run resulting in a displacement in the final density profiles.

From the dye front photographs sketches were made of the dye fronts in non-dimensional coordinates for comparison between the two lake models. The vertical coordinate of the side view sketches were non-dimensionalized with the appropriate length sclaes used in the particular overall Richardson numbering compared. The sketches recorded the shape of the dye front at specific downstream distances and time after the inflow was initiated. The recorded times were non-dimensionalized by multiplying t, the photographed time after initial inflow by Q/Vol. where Q is the flowrate and Vol. represents the volume of the lake. Spacial and temporal distribution characteristics of the inflow into the stratified lake were thus examined.

In order to investigate the Richardson and Reynolds number dependence, the Richardson parameter ratio, $\frac{\bar{J}_{iS}}{\bar{J}_{iL}}$, was plotted against the Reynolds number ratio, $\frac{Re_S}{Re_L}$, for each pair of tests in the shallow and deep lake models. The subscripts S and L indicate small or shallow and large or deep lake model. Each point on the plot was then categorized and appropriately marked according to the degree of similarity between the top views. On another copy of the plot the same was done for the side views. Because there are different possible definitions for the

overall Richardson parameter $\overline{J}_i$, this procedure was repeated for other Richardson parameter ratios.

If the Reynolds number is large enough, the flow will have a weak dependence on Reynolds number, and points marked for similarity agreement between pairs tests will extend over a wide range of Reynolds number ratios. If there is the expected strong dependence on Richardson number these same points should be located in a narrow band of Richardson parameter ratios.

In addition, if the Reynolds number and the Richardson number adequately describe the flow situation in the presence of geometric distortion, these points marked to show similarity agreement will occur in well defined zones. Preferably these zones would be located around $\frac{Re_S}{Re_L} = 1$ and $\frac{\overline{Ji}_S}{\overline{Ji}_L} = 1$. These conditions on any plot would imply that the Reynolds number and overall Richardson number have been properly defined for modeling fluid inflows into stratified lakes using vertical scale distortion.

Thus there are three main features to look for in the plots: (1) the shape and location of general regions where similarity between paired tests exists, (2) how clearly defined these regions are, and (3) agreement with the similitude assumptions incorporated in the original test design.

CHAPTER IV

EXPERIMENTAL RESULTS

The Richardson number (one of the several expressions for $\overline{J}$) and the Reynolds number form the basis for the similarity criteria to be used in modeling fluid inflows into stratified lakes. The two basic means of comparing the similarity between two test runs are density distributions and dye front profiles. These can be further divided into initial and final density distribution profiles plotted from conductivity probe measurements, and top and side view dye front profiles photographically recorded during an experiment.

Density Profiles

Figure 5 presents the initial density profiles prior to the test runs, S-16 and L-16. These are plotted in terms of a normalized non-dimensional density, $\rho^* = \frac{\rho - \rho_2}{\rho_3 - \rho_2}$, and a non-dimensional vertical coordinate, $\frac{z}{H}$. It can be seen from Figure 5 that these two initial profiles are very close to the same shape with about the same slope through the mid-region. The final density distribution profiles taken after the test runs are shown in Figure 6. The discrepancy in the relative positions of the final profiles is due primarily to the difference in the proportions of the intermediate inflow density over the density difference in the lake. The depth-wise final distribution profile of lower ρ^* values indicates relatively more mixing with the lighter upper fluid

as the flow entered the lake. A variety of initial density distribution profiles were compared in order to determine their relationship in producing similar inflow distributions. While the density profiles were not intended to be a strict basis for judging similarity between test runs, they did provide additional information for producing similarity between test runs. It was found that in general for the tests showing similarity in the side view profiles, that the final density distribution profiles were also reasonably similar.

Dye-Front Profiles and Comparison Criteria

The chief means of determining the amount of similarity achieved between flow patterns on the two lakes is the comparison of dye-front profiles. For each test run, the vertical coordinate of the side view dye front profiles was non-dimensionalized with the depth of the lake (H). These side view profiles were compared for tests matching in overall Richardson numbers $\overline{J}_1$ or $\overline{J}_2$ since H is the vertical length scale used in both these parameters. But for tests matching in overall Richardson numbers $\overline{J}_3$ or $\overline{J}_4$ which employ the diffusion layer thickness (D) as the vertical length scale, the vertical coordinate in the side view profiles should be non-dimensionalized with D instead of H. If the ratio of diffusion layer thicknesses $\frac{D_S}{D_L}$ is equal to the ratio of the depths $\frac{H_S}{H_L}$, then either D or H may be used to non-dimensionalize the vertical coordinate. When $\frac{D_S}{D_L}$ largely differed from $\frac{H_S}{H_L}$ for tests matched in $\overline{J}_3$ or $\overline{J}_4$, the similarity judgement was made on the side view profiles where the vertical scale was $\frac{z}{D}$.

There is a problem of which vertical height to use in the side view profiles when the tests are matched in $\overline{J}_5$ or $\overline{J}_6$. Since both these

overall Richardson numbers use D and H, choosing the appropriate one for non-dimensionalizing the vertical coordinate in the side view profiles is difficult. This problem can be circumvented by scaling D the same as H. In most tests $\frac{D_S}{D_L}$ did not differ from $\frac{H_S}{H_L}$ enough to effect the similarity of the profiles.

Figure 7 is an enlarged side view portion of test run photographs for tests S-16 and L-16 small and large lake runs respectively. From these photographs non-dimensional side view profiles were sketched for test S-16 shown in Figure 8 and for test L-16 in Figure 9. Side view sketches at several different downstream positions were usually made for each test run in this manner. Since there was no horizontal distortion, the top views of the lakes were compared from the photographs. In the top view sketches the lateral coordinate from the center line of the lake was non-dimensionalized with the half-width of the lake.

In comparing either top or side dye front profiles between the two lakes, the size of the non-dimensional dye-front profiles was the most important consideration in determining relative similarities between test runs. The shape and taper of the dye front was also considered but to a lesser extent. One of four different degrees of similarity were used to describe either top or side view comparison of each small lake run to every other large lake run. Briefly these four are: (1) very similar - dye fronts are congruent in size, shape and taper, (2) similar - close to the same size, shape and taper, (3) somewhat similar - sizes vary by less than a factor of two, and (4) dissimilar - sizes differ by more than a factor of two.

Figure 10 shows the top view dye front profiles of test runs S-17 and L-10. These profiles are judged to be similar. In this case and

in simulating top views in general, it was found that by matching the overall Richardson number, $\overline{J}_1 = \frac{g\Delta\rho\ell^2}{\rho_c V_i^2 H}$, good agreement between top dye front profiles could be obtained. For tests S-17 and L-10: $\overline{J}_1 \simeq 800$ and Re $\simeq$ 3300.

Contrasting this good agreement are the top view sketches of Figure 11 which show dissimilarity between test runs S-16 and L-16. These tests had different values for $\overline{J}_1$, but were matched fairly well for the overall Richardson number $\overline{J}_6 = \frac{g\Delta\rho H}{\rho_c V_i^2 D}$. For tests S-16 and L-16; Re = 2624 and 5313 respectively, while the value of $\overline{J}_6$ was approximately 0.7 for both tests. Since the dispersion patterns are distinctly dissimilar, the overall Richardson number $\overline{J}_6$, must be considered inadequate as modeling criteria, from top view dye trace record.

The side view profiles for tests S-16 and L-16 can be plotted using either $\frac{z}{H}$ or $\frac{z}{D}$ for the vertical coordinate since the diffusion layer thickness was the same proportion of the depth for both tests. The side view profiles are plotted in $\frac{z}{H}$ in Figure 12 and in $\frac{z}{D}$ in Figure 13. It can be seen in both plots that the profiles are similar, but the inflow has sought a different height in each run. Consequently, the side view dye front profiles are displaced. Just as the final density profiles are displaced, so the side profiles are displaced and most likely because the intermediate density of the inflows were not the same proportion of the density differences in the lakes. This discrepancy in the displacement of the lenses is not judged to be a serious factor in determining the similarity between the side view profiles. Nor was the discrepancy in the vertical displacement of the lenses expected to cause major effects in the top view profiles due to the lower lens lifting off at the wider portion of the contour. The

similarity of these profiles and in other side view comparisons where the values of $\overline{J}_6$ on either lake were matched indicate the success of that Richardson parameter in modeling side view dye front profiles.

Figure 14 shows the side view profiles of tests S-17 and L-10 which were matched in $\overline{J}_1$ values. Here the dissimilarity between the profiles represents the inadequacy of the overall Richardson parameter to produce successful modeling of the side view dye front traces.

One phenomenon that was observed in the top view of the lakes was a flow instability of the inflow progressing through the lake. This instability manifest itself as a lateral back and forth motion of the inflow moving through the lake and eventually forming eddies at the bends. These eddies grew as large as the width of the lake. The experiments were constrained so that the effects of this instability were negligible in simulating the inflow distribution in the lake.

Similarity Parameters

In order to determine which of the six non-dimensional parameters was the most appropriate overall Richardson number, plots of Richardson number ratio versus Reynolds number ratio were made for each set of data between the two lakes. Richardson parameter $\overline{J}_5$ was soon eliminated since it produced the worst similarity criteria in the lake tests and will not be considered further in the discussion of the results. Two plots of Richardson number ratio versus Reynolds number ratio were made for each of the remaining five Richardson parameters. In one set each point was given the appropriate marking corresponding to the degree of similarity achieved in the top view comparisons and likewise the other set was marked for side view comparisons.

Circles, triangles and squares are used to denote dissimilar, somewhat similar and similar test runs respectively. These plots were also designed to help understand the modeling dependence on Richardson and Reynolds number.

Each plot of Richardson parameter ratio versus Reynolds number ratio was examined with respect to the three features previously mentioned. The location and shape of the regions of similarity depend upon which view, top or side, is under consideration.

In comparing the five plots marked for top view similarity, Figures 15-19, it is seen that the regions of similarity are about the same for Richardson parameter ratios $\frac{\bar{J}_{1S}}{\bar{J}_{1L}}$ and $\frac{\bar{J}_{3S}}{\bar{J}_{3L}}$, that is around $\frac{\bar{J}_{iS}}{\bar{J}_{iL}} \simeq 1$. Similarity around Richardson parameter ratios of about 1 imply that this particular Richardson parameter can be used as successful modeling criteria.

The regions for top view similarity for $\frac{\bar{J}_{2S}}{\bar{J}_{2S}}$, $\frac{\bar{J}_{4S}}{\bar{J}_{4L}}$ and $\frac{\bar{J}_{6S}}{\bar{J}_{6L}}$, Figures 16, 18 and 19, are located somewhat below $\frac{\bar{J}_{iS}}{\bar{J}_{iL}} \simeq 0.5$. Here the difference between the two groups stems from the scaling of the velocity gradient. In $\bar{J}_1$ and $\bar{J}_3$ the velocity gradient was scaled with the inlet velocity and a horizontal length, while for $\bar{J}_2$, $\bar{J}_4$ and $\bar{J}_6$ the velocity gradient was scaled with a depth in the lake. The scaling of the density gradient accounts for the differences within each of these two groups. $\bar{J}_1$ and $\bar{J}_2$ differ from $\bar{J}_3$, $\bar{J}_4$ and $\bar{J}_6$ respectively in that the former scales $\partial\rho/\partial z$ with $\Delta\rho/H$ and the latter scales $\partial\rho/\partial z$ with $\Delta\rho/D$.

Based on location of the regions of top view similarity, the plots $\frac{J_{1S}}{J_{1L}}$ and $\frac{J_{3S}}{J_{3L}}$ are most informative since they agree best with similitude assumptions incorporated in the original test design. There is a

problem in determining which of the two plots $\frac{J_{1S}}{J_{1L}}$ or $\frac{J_{3S}}{J_{3L}}$ yields the best results. Since on neither plot is the similarity more clearly defined than on the other, the final selection was based on the nearness of the three similarity points to the Richardson parameter ratio $\frac{J_{iS}}{J_{iL}} = 1$. From this, $\overline{J}_1$ is selected as the best overall Richardson number from top view comparisons.

The situation is reversed when examining the plots where the side view similarity of dye front profiles is considered (Figures 20-24). Here the plots of $\frac{J_{2S}}{J_{2L}}$, $\frac{J_{4S}}{J_{4L}}$ and $\frac{\overline{J}_{6S}}{J_{6L}}$ locate the similarity regions closer to $\frac{J_{iS}}{J_{iL}} = 1$. The choice between these two plots is obvious. The plot of $\frac{J_{6S}}{J_{6L}}$ (Figure 24) clearly locates the side view similarity region closer to $\frac{J_{iS}}{J_{iL}} = 1$ which is the best agreement with the similitude assumptions of the original test design. Again choosing which plot more clearly defines the region of similarity is a problem, but $\frac{J_{6S}}{J_{6L}}$ does seem to be better defined in that the region is clustered closer together at a higher Richardson parameter value.

The fact that not any of the plots for any of the Richardson parameters show the same regions of similarity for the top views as for the side views clearly indicates that no single Richardson parameter investigated plus Reynolds number form a complete similarity criteria for the entire flow situation. One of the important effects of vertical scale distortion then must be that the lateral dispersion is affected differently than the vertical diffusion. The overall dispersion is a combination of diffusion (molecular and turbulent) and convection (convection caused by the velocity variations in the entire cross section).

Molecular diffusion can be considered negligible for this open channel flow situation.

The dominant mechanism in the lateral dispersion process is the lateral variations in the convective velocity. This is indicated by the similarity between top view profiles of tests matched by $\overline{J}_1$ in which the velocity gradient was scaled with a horizontal length. The turbulence has relatively little affect on lateral dispersion as reported by Miller and Richardson (11).

Turbulent eddies are the dominant mechanism in the diffusion process. The side view profiles provide a comparison for the mixing process of turbulent diffusion between test runs. While turbulent diffusion and convection are not completely independent processes, they do dominate in different aspects of dispersion. More important is that by exaggerating the vertical scale these mechanisms are affected differently.

In studying the shape of the regions of similarity for both top and side views, it is seen that contrary to the expected weak Reynolds number dependence and strong Richardson number dependence, the plots actually indicate a more or less equal dependence on both parameters. The Reynolds number ratios in the top view region of similarity differ from the Reynolds number ratios for the side view region of similarity. This was primarily due to the large diffusion layer thickness needed in the deeper lake to produce a correspondingly thick side view profile.

There are several reasons for the lack of clarity in defining the regions of similarity for either top or side views. First is a lack of points in certain areas in and around the similarity zones. In some cases the limitations of the flow facilities prevented certain

test configurations needed to produce points in these zones. Although the plots clearly indicate that one Richardson number parameter is insufficient to represent the entire flow problem, the lack of well-defined regions of similarity must cause concern over the inadequacies of such grossly simplified definitions of overall Richardson numbers.

CHAPTER V

CONCLUSIONS

The conclusions from this experimental investigation may be listed as follows:

1. Two parameters (i.e., a single Richardson number expression and a Reynolds number) are not enough to adequately describe the entire flow situation. Two expressions for an overall Richardson number were necessary to simulate side and top view of flow fields.

2. Based on the top view profiles the expression for an overall Richardson number which produced the best flow simulation was $\overline{J}_1 = \frac{g\Delta\rho\ell^2}{\rho V_i^2 H}$. This implies that the vertical velocity gradient scales with a horizontal length when horizontal dispersion is being considered.

3. The best flow simulation between side view profiles was produced through a different expression for the overall Richardson number, $\overline{J}_6 = \frac{g\Delta\rho H^2}{\rho V_i^2 D}$. Here the vertical velocity and density gradients are scaled with the depth of the lake and the diffusion layer thickness respectively.

4. From the above it must be concluded that distorting the vertical scale does in fact affect lateral dispersion differently than it affects vertical diffusion. And the modeling geometry will largely determine the extent of this discrepancy. This was predicted by Fisher and Holley (5), but in failing to consider the effects of a density

gradient their analysis of the relative magnitudes of the effects that vertical scale distortion has on diffusion and dispersion is very limited.

5. The dependence of the flow on Reynolds number is not as weak as expected nor is the flow as strongly dependent on Richardson number as expected.

Even though distorting the vertical scale affected horizontal dispersion and vertical diffusion to different degrees, certain aspects of the flow could be modeled by choosing the appropriate criteria as has been shown.

SELECTED BIBLIOGRAPHY

(1) Barr, D. I. H. "Model Simulation of Vertical Mixing in Stratified Flowing Water." The Engineer, Vol. 215, No. 5587 (February 22, 1963), 345-352.

(2) Barr, D. I. H. "Densimetric Exchange Flow in Rectangular Channels." Part III. La Houille Blanche, Vol. 6 (1967), 619-631.

(3) Browand, F. K., and C. D. Winant. "Laboratory Observations of Shear Layer Instability in Stratified Fluid." Submitted for publication in the Journal of Geophysical Fluid Dynamics, 1972.

(4) Ellison, T. H., and J. S. Turner. "Turbulent Entertainment in Stratified Flows." J. Fluid Mechanics, Vol. 6, pt. 3 (1959), p. 423.

(5) Fischer, H. B., and E. R. Holley. "Analysis of the Use of Distorted Hydraulic Models for Dispersion Studies." Water Resources Research, Vol. 7, No. 1 (February, 1971), 46-51.

(6) Francis, J. R. D. "Scaling in River and Estuary Models." Engineering, Vol. 190 (September, 1960), 329-331.

(7) Gibson, C. H., and W. H. Schwarz. "Detection of Conductivity Fluctuations in a Turbulent Flow Field." Journal of Fluid Mechanics, Vol. 16 (1963), 357-363.

(8) Hutchison, G. E. A Treatise on Limnology. Vol. 1. New York: John Wiley and Sons, Inc. London: Chapman and Hall, Ltd., 1957.

(9) Keulegan, G. H. "The Mechanism of an Arrested Saline Wedge." Estuary and Coastline Hydrodynamics. New York: McGraw-Hill, 1966.

(10) Long, R. R. "A Theory of Turbulence in Stratified Fluids." J. Fluid Mechanics, Vol. 42, pt. 2 (1970), 349-365.

(11) Miller, A. C. and E. V. Richardson. "Diffusion and Dispersion in Open Channel Flow." A.S.C.E. J. of the Hydraulics Division, HY 1 (January, 1974), 159-171.

(12) Morton, B. R. "Forced Plumes." J. Fluid Mechanics, Vol. 5 (1959), 151-163.

(13) Thorpe, S. A. "Experiments on the Instability of Stratified Shear Flows: Miscible Fluids." J. Fluid Mechanics, Vol. 16, pt. 2 (1971), 299-319.

(14) Thorpe, S. A. "Experiments on Instability and Turbulence in a Stratified Shear Flow." J. Fluid Mechanics, Vol. 61, pt. 4 (1973), 731-751.

(15) Vogel, S. J. "Similitude Investigation of Vertical Exaggeration in Stratified Lake Models." (unpub. M.S. thesis, Oklahoma State University, 1972.)

APPENDIX A

CONDUCTIVITY PROBE

CONDUCTIVITY PROBE

The conductivity probe was made by hand by first drawing a 3 mm outside diameter flint glass tube down to an approximate inside diameter of 0.002 inch. Then the platinum wire was threaded into the tube. Once threaded, the tube was reheated and shaped also sealing the platinum wire inside.

The tip was carefully shaped with fine sand paper then coated with platinum black using a standard plating solution. A 5 mm o.d. flint glass tube epoxied to the smaller tube provided the body for the probe. Figure 22 is a diagram of the probe and electrical network.

The probe tip was used as one electrode and a wire mesh screen as the other. Then immersing both in a salt water solution completed the circuit of an A.C. impedance bridge. In this way the local resistance of the solution at the probe tip was measured. By measuring the resistivity of several salt solutions over a range of density, a calibration chart of resistivity versus density was plotted. To measure a particular density profile, several resistivity readings were made at various depths then converted to densities and plotted against depth to produce a profile.

APPENDIX B

FIGURES AND TABLE

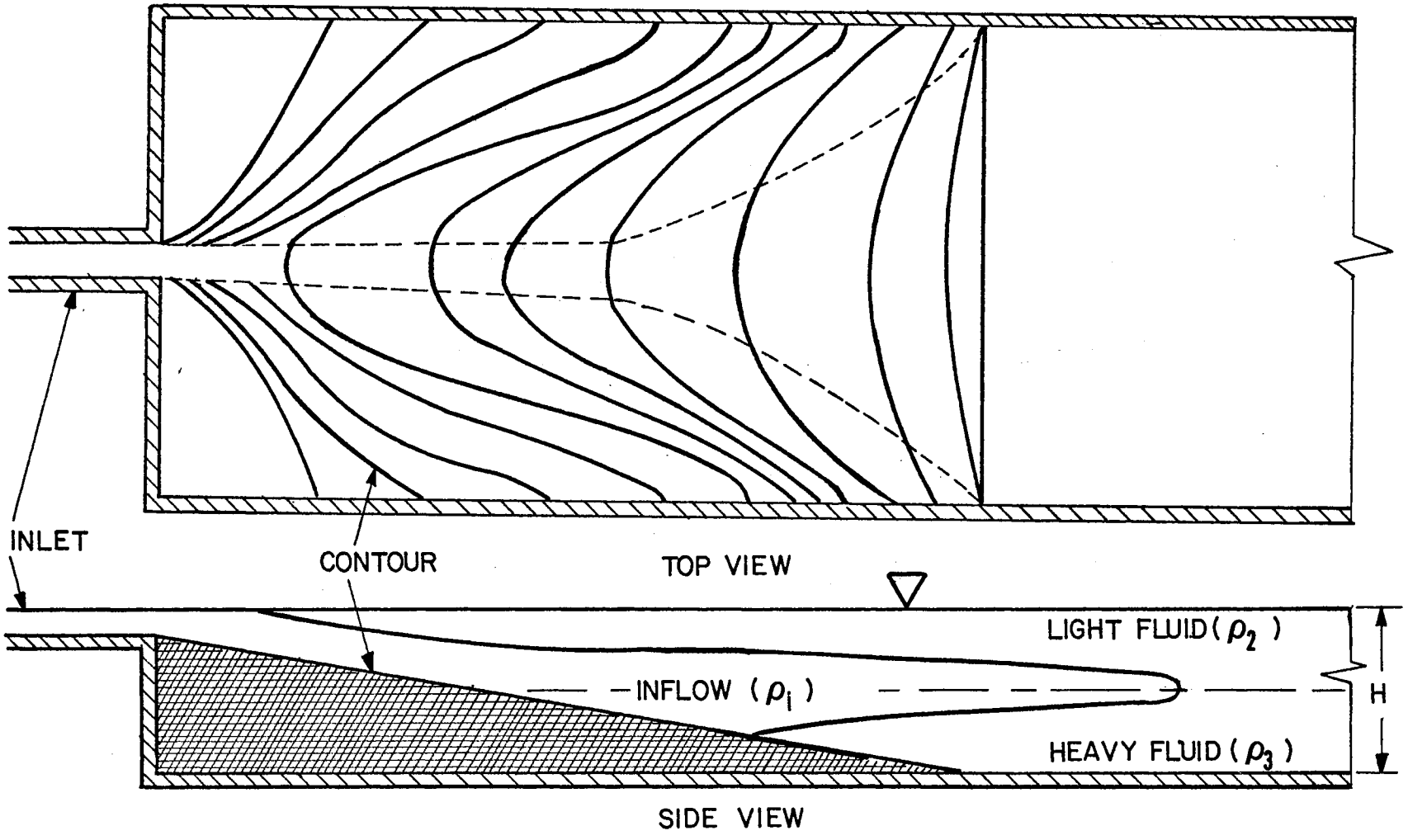

Figure 1. Sketch of the Physical System Being Modeled

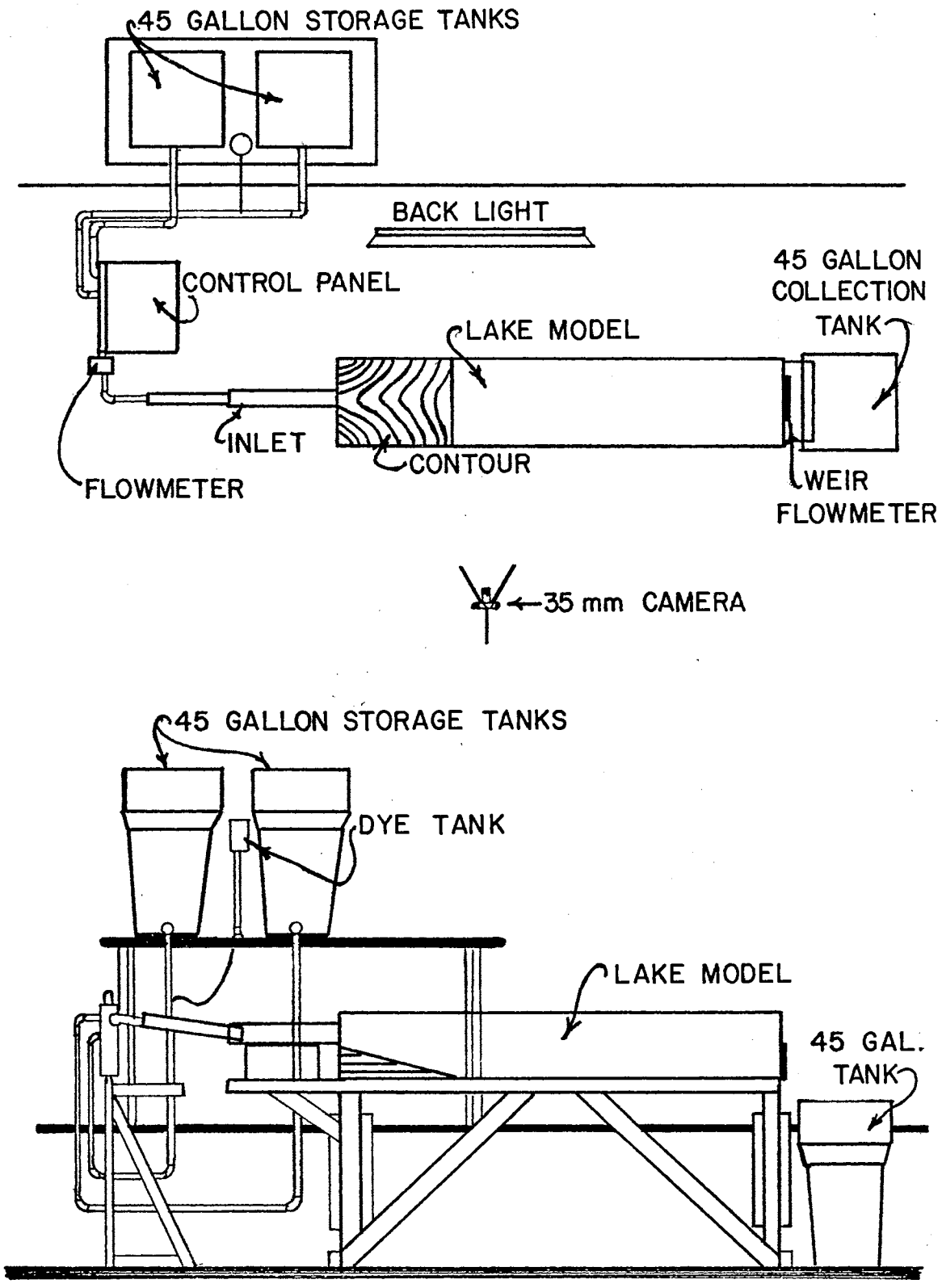

Figure 2. Lake Model and Inflow System

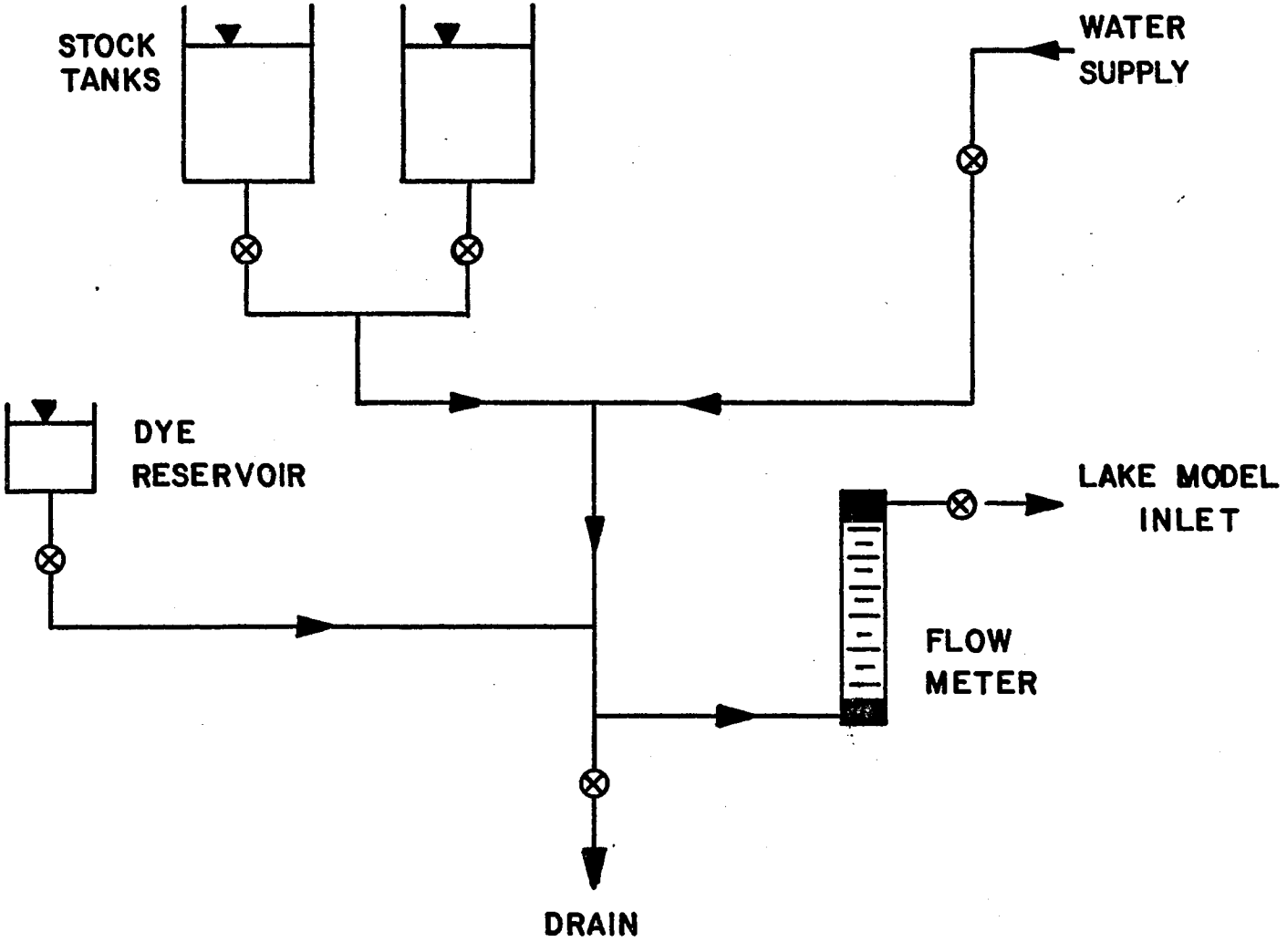

Figure 3. Schematic of Hydraulic System

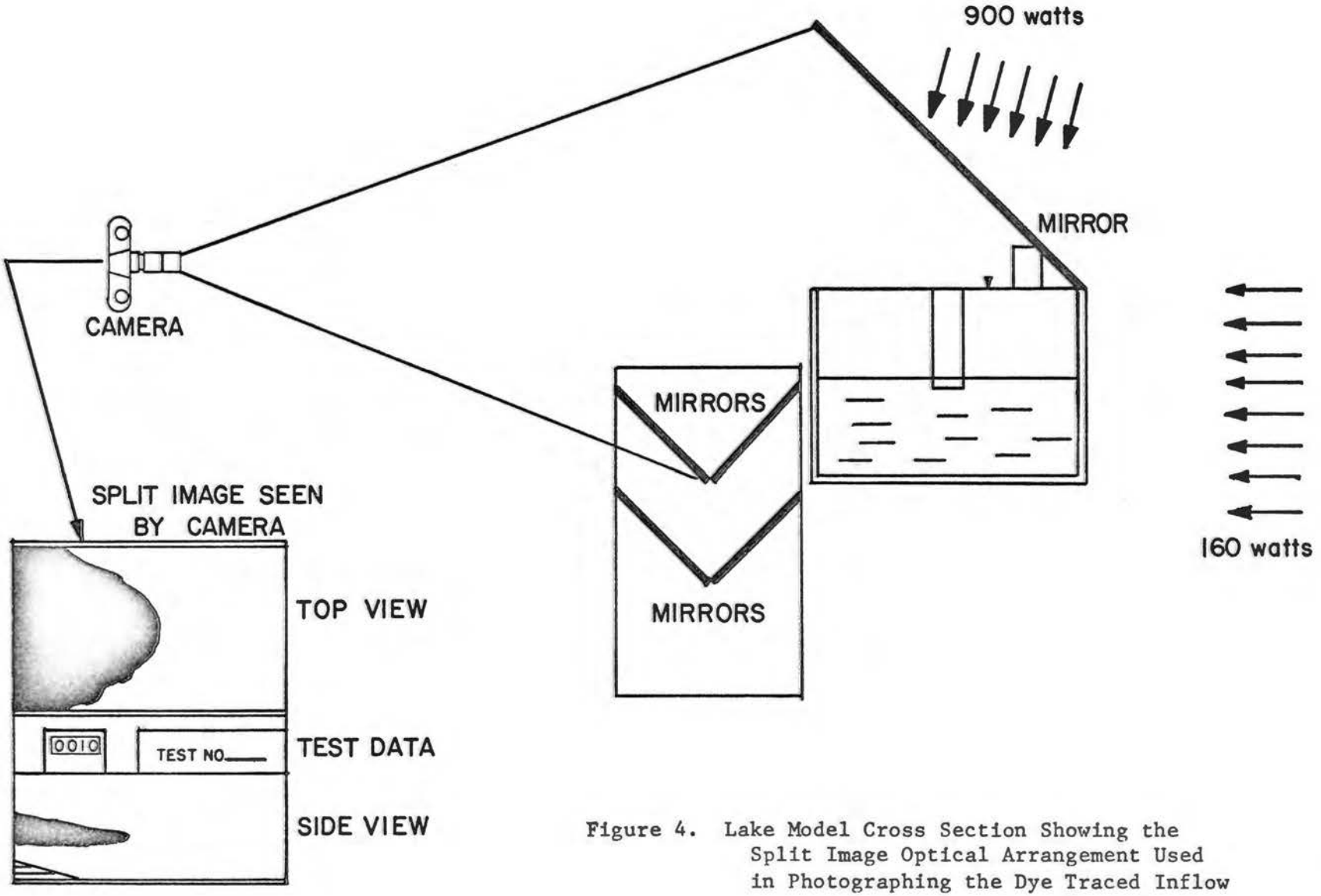

Figure 4. Lake Model Cross Section Showing the Split Image Optical Arrangement Used in Photographing the Dye Traced Inflow

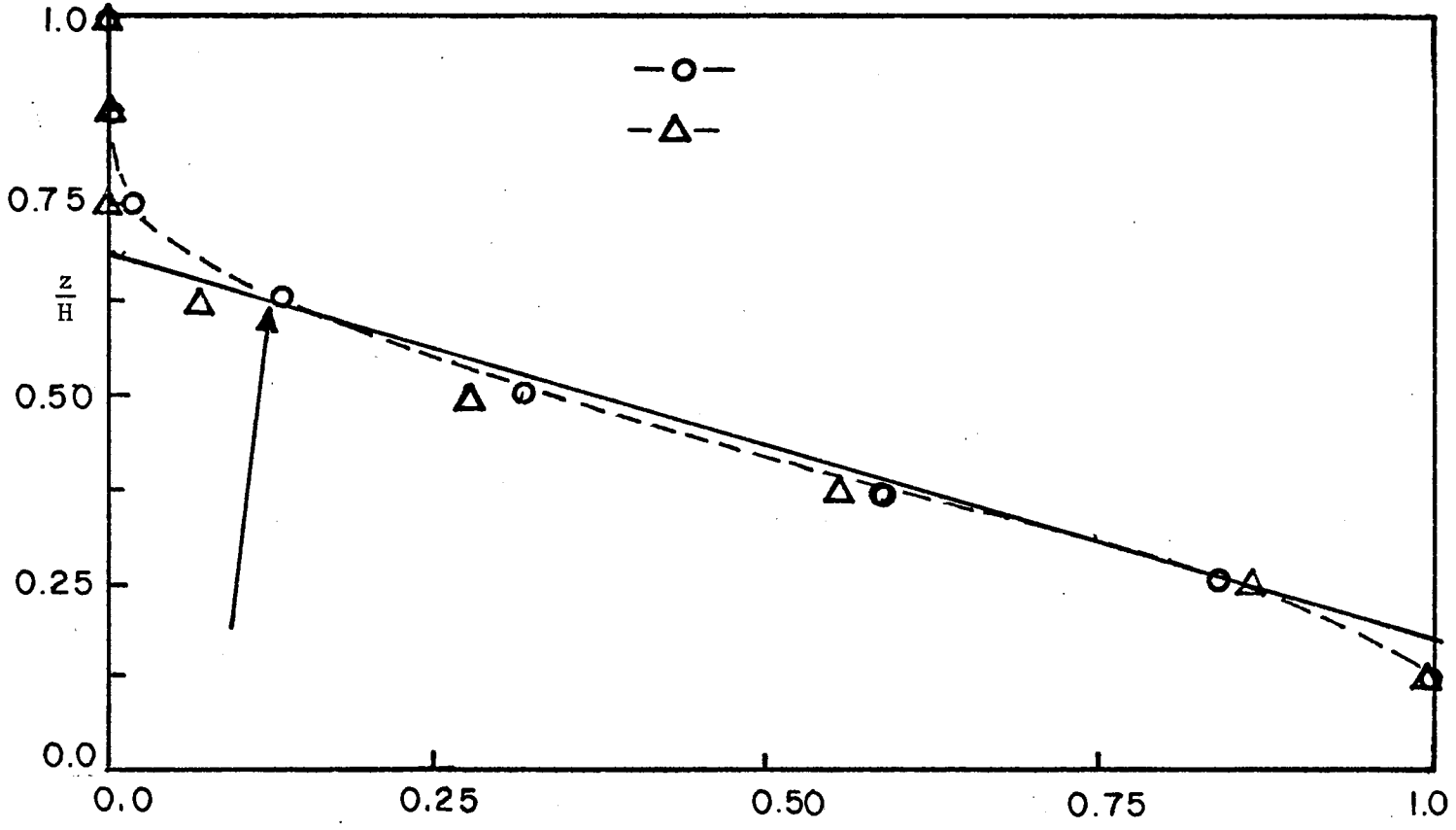

Figure 5. Comparison of Initial Density Profiles

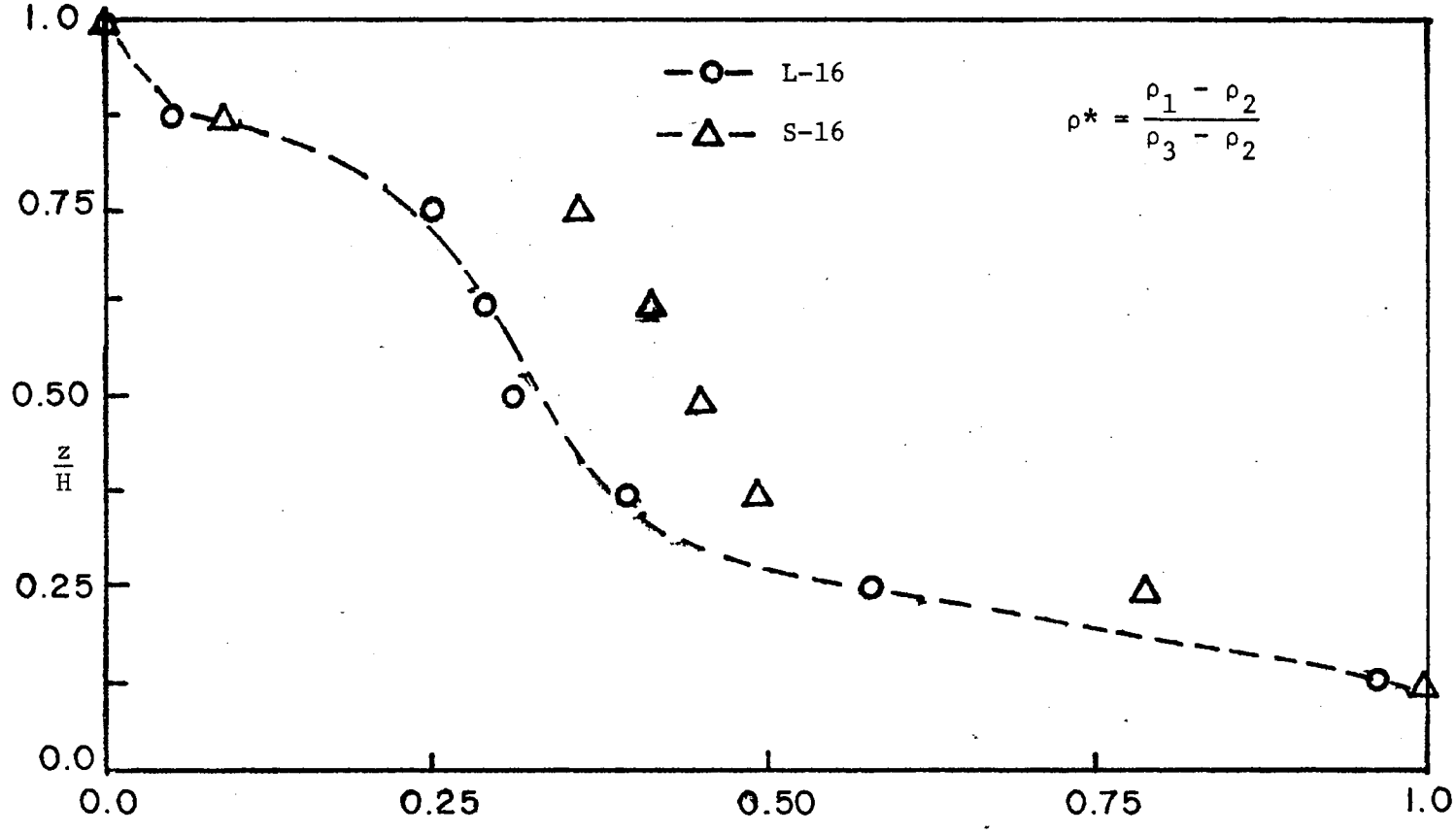

Figure 6. Comparison of Final Density Profiles

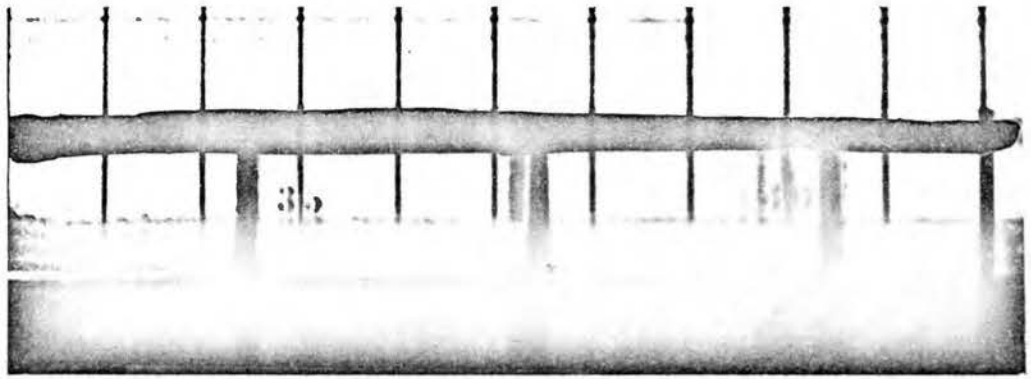

Test S-16

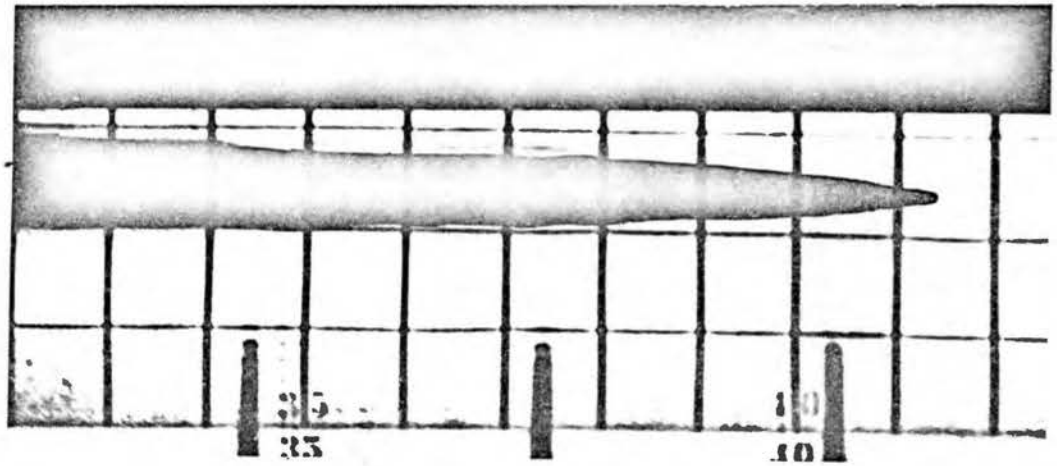

Test L-16

Figure 7. Side View Photographs

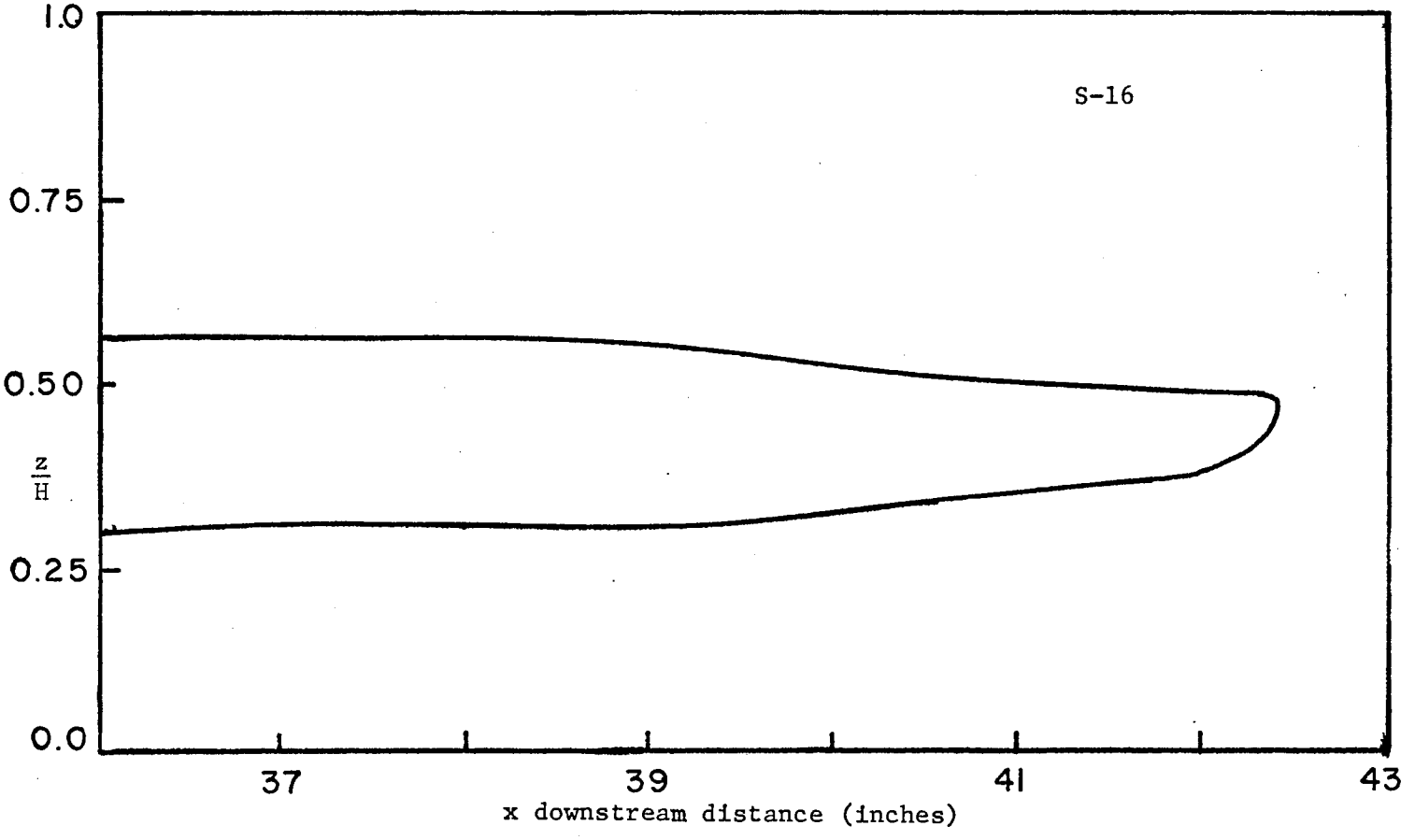

Figure 8. Side View Dye Front Sketch Test S-16

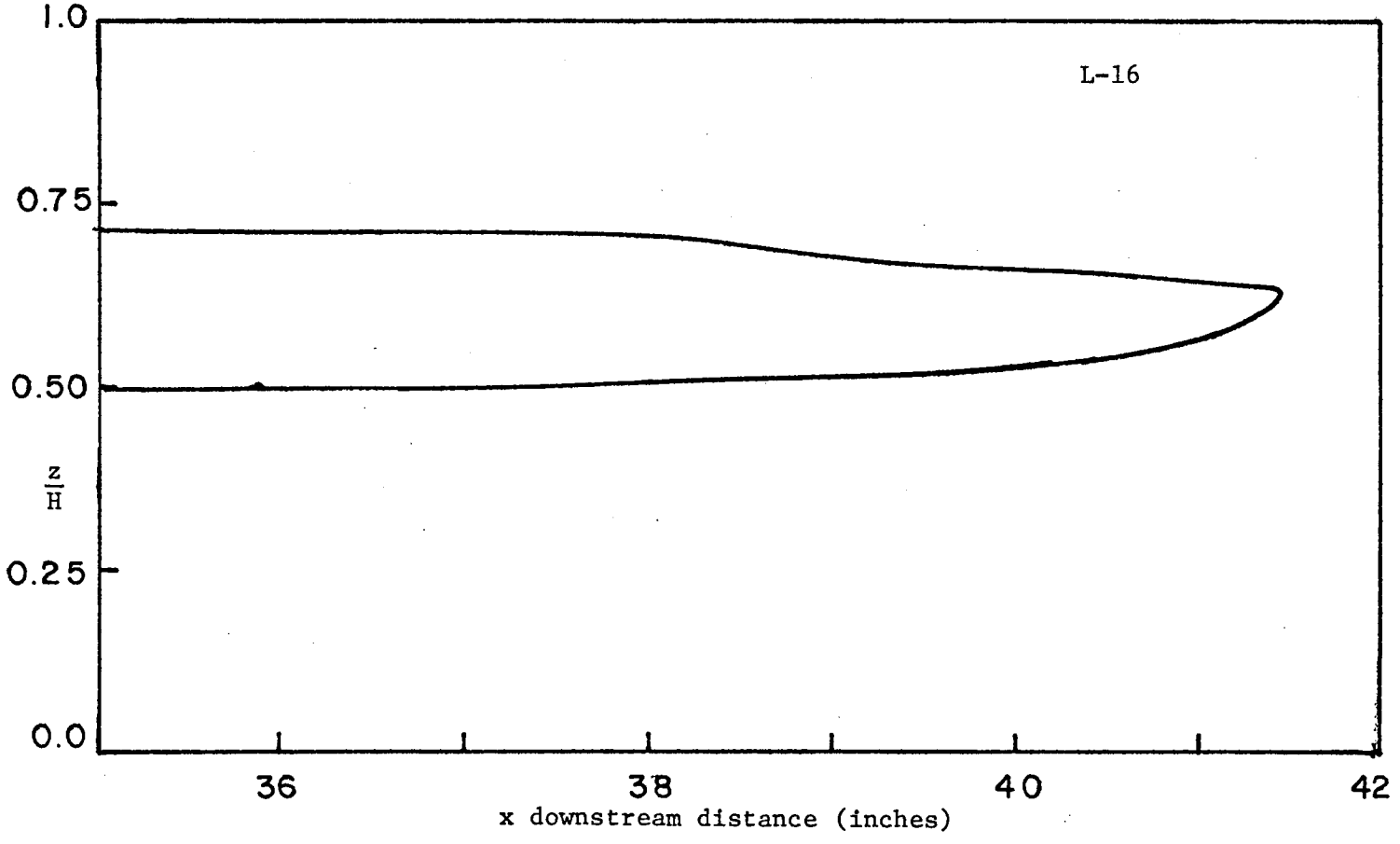

Figure 9. Side View Dye Front Sketch Test L-16

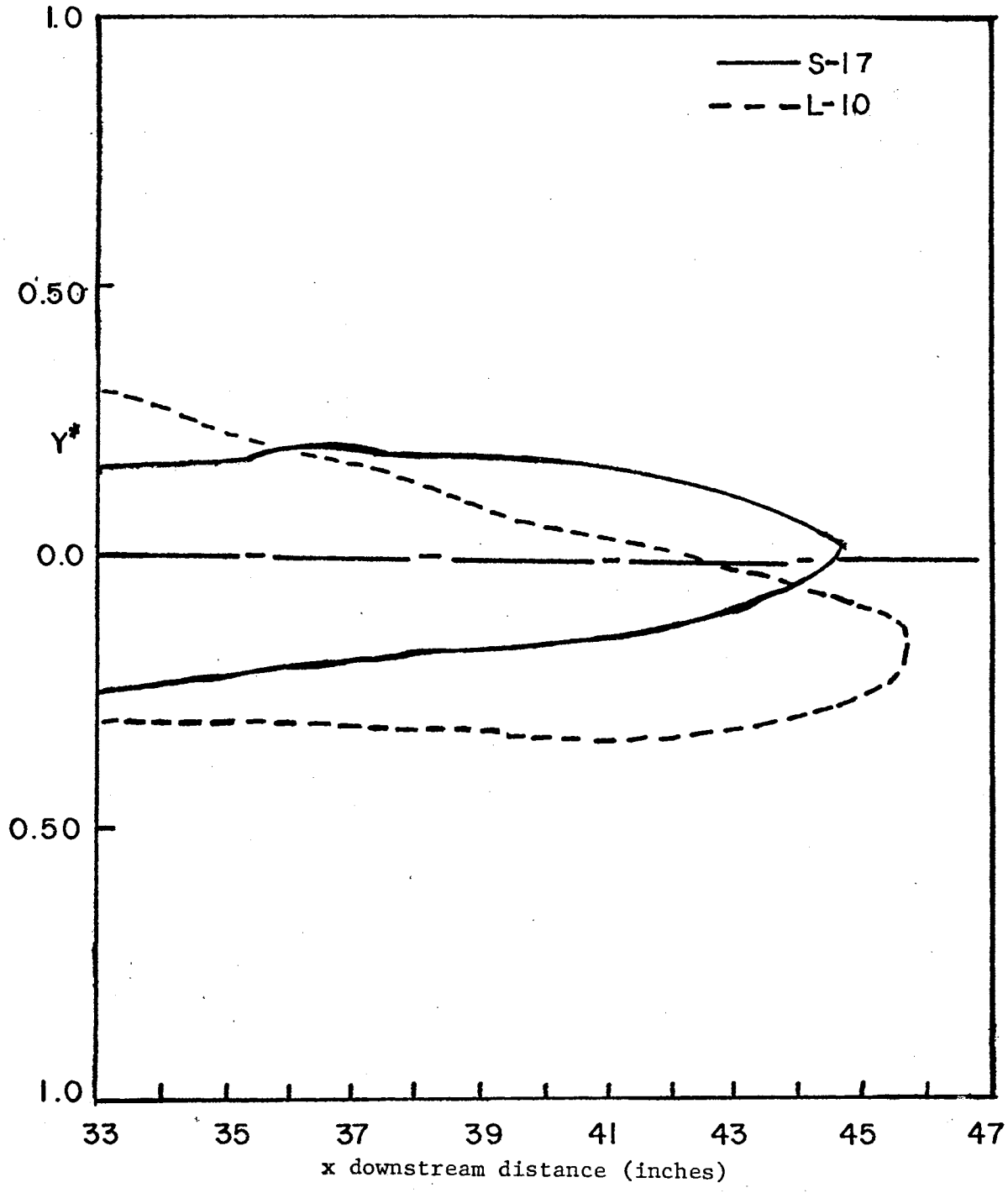

Figure 10. Top View Comparison of Dye Traces
Tests S-17 and L-10

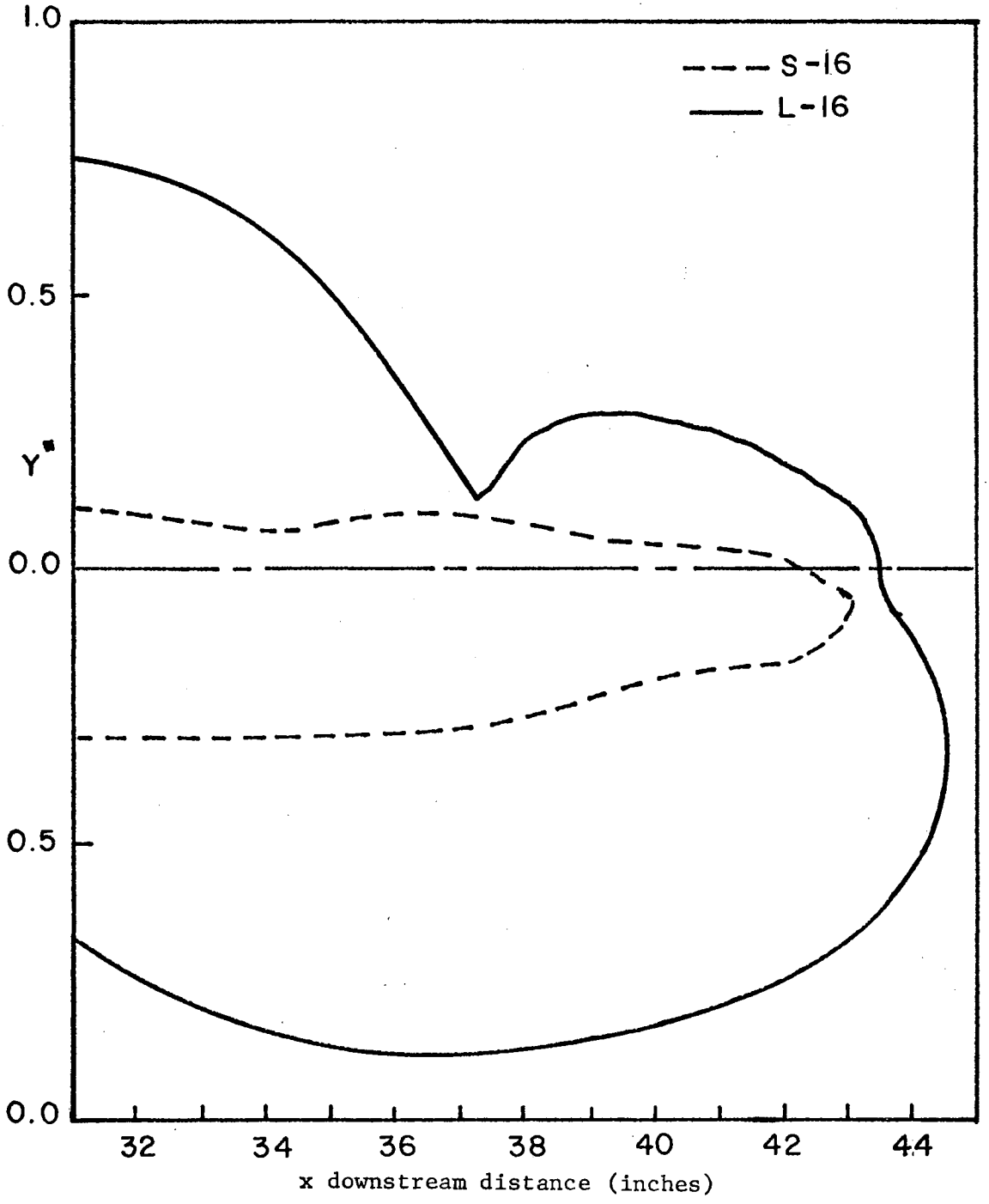

Figure 11. Top View Comparison of Dye Traces
Tests S-16 and L-16

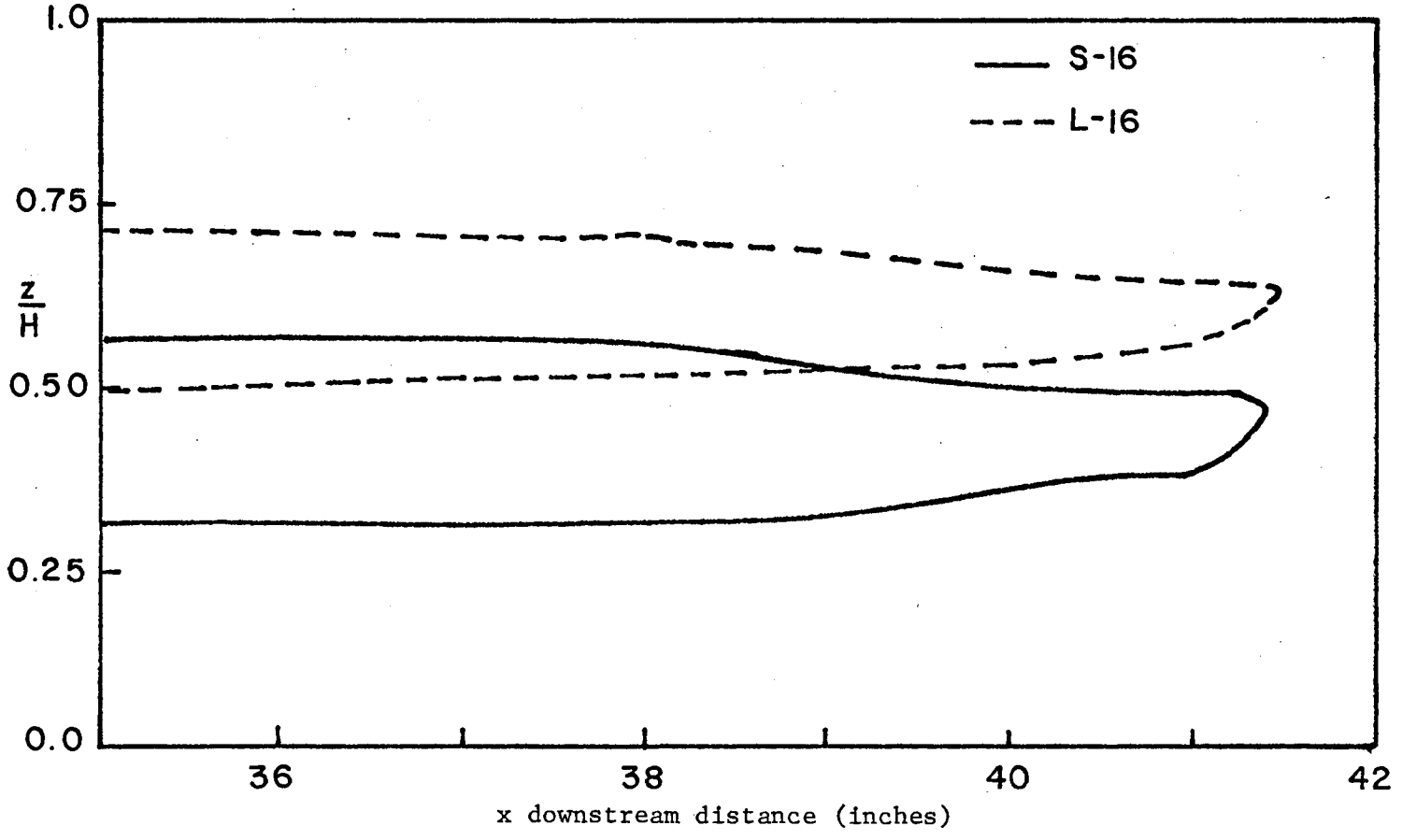

Figure 12. Side View Comparison of Dye Traces Tests S-16 and L-16 $\frac{z}{H}$

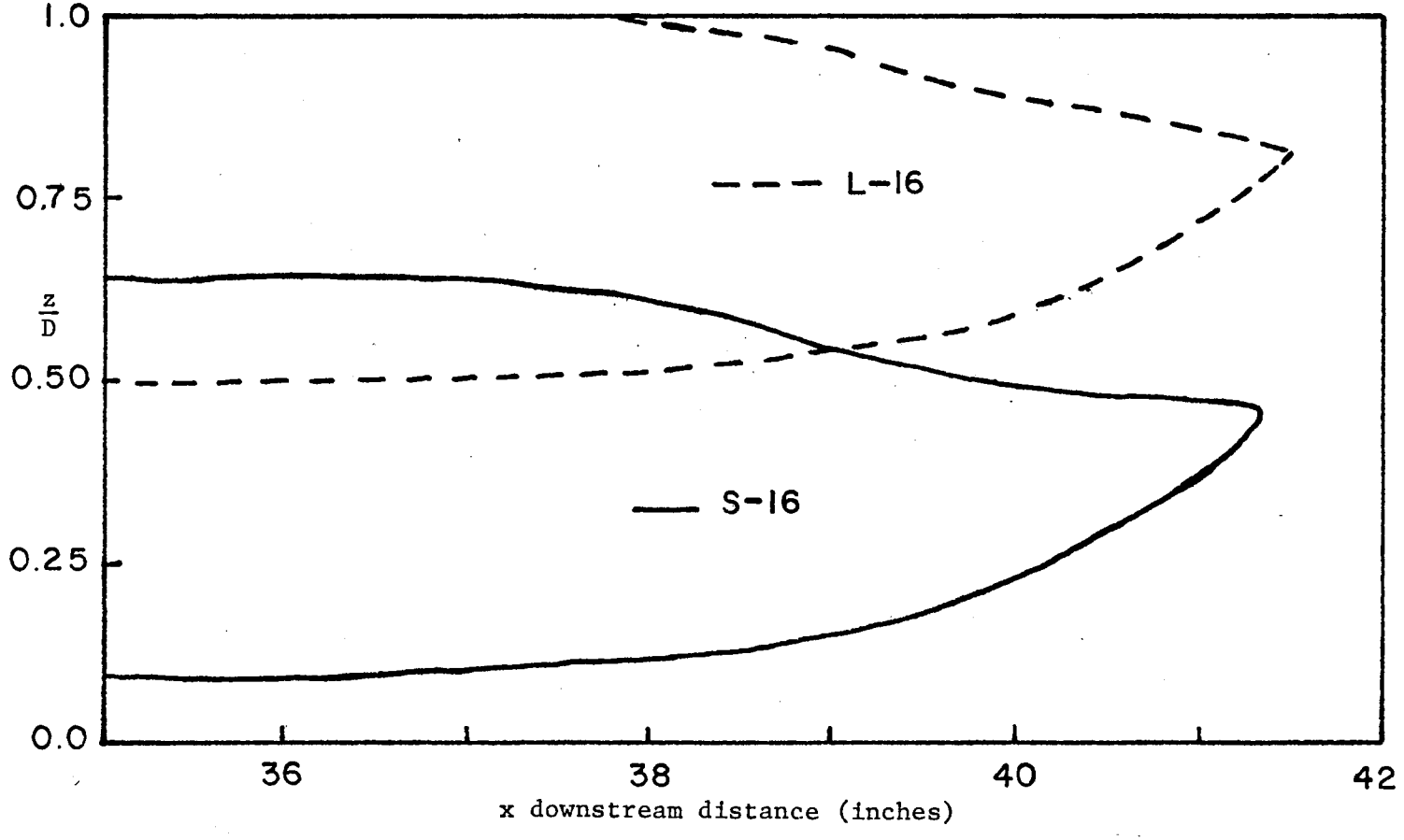

Figure 13. Side View Comparison of Dye Traces Tests S-16 and L-16 $\frac{z}{D}$

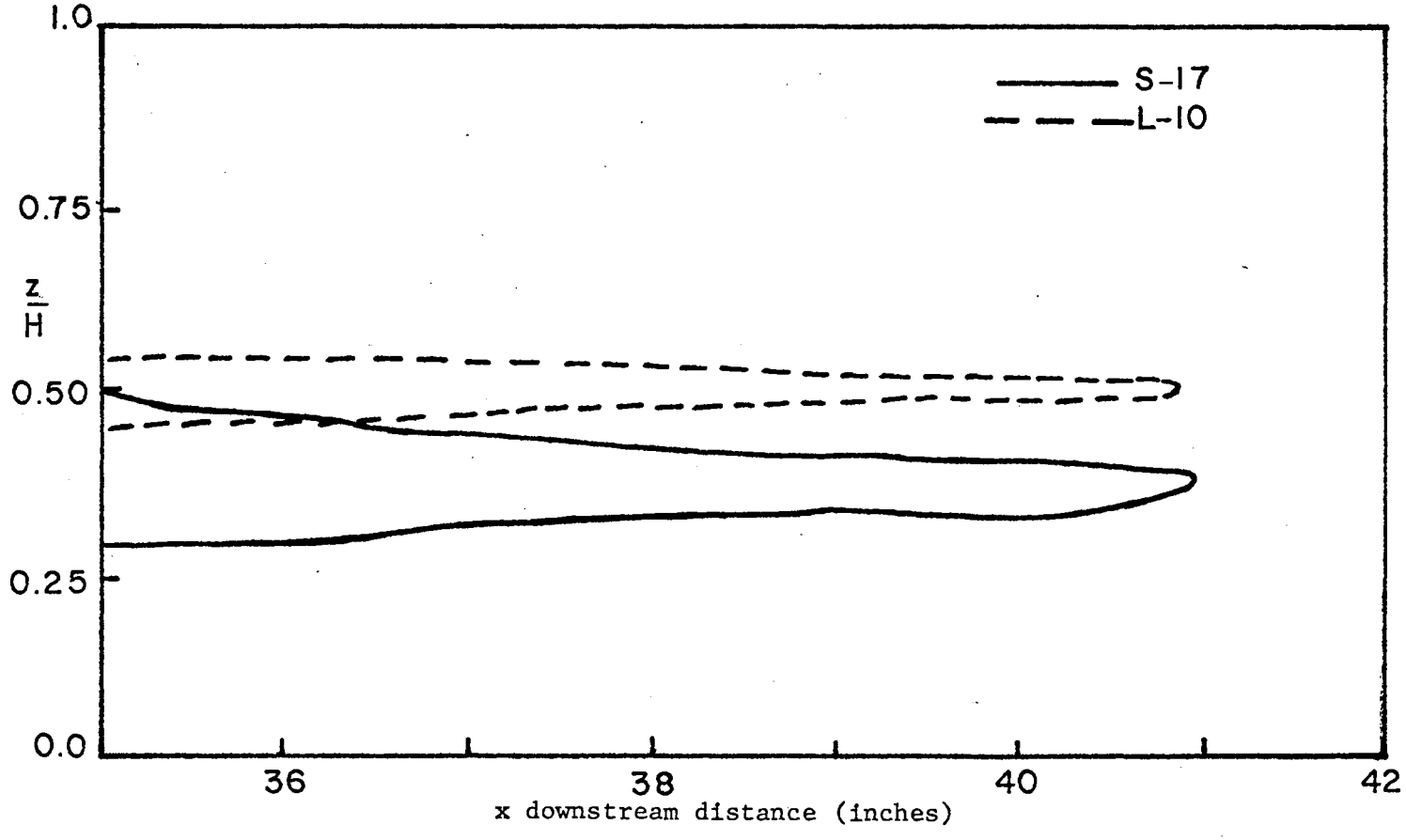

Figure 14. Side View Comparison of Dye Traces Tests S-17 and L-10

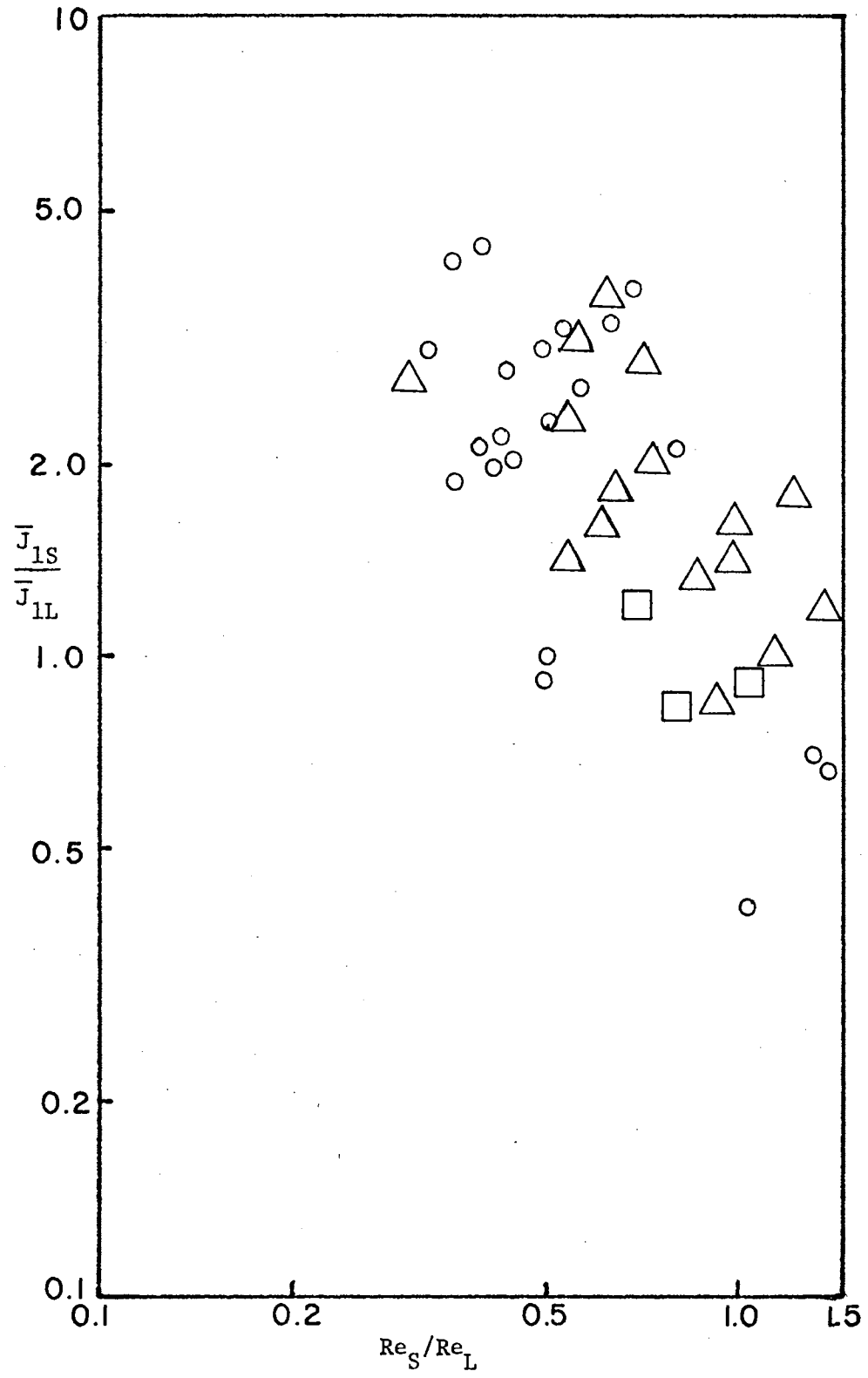

Figure 15. Richardson Parameter Ratio (1) vs. Reynolds Number Ratio. Points are Marked for Top View Similarity

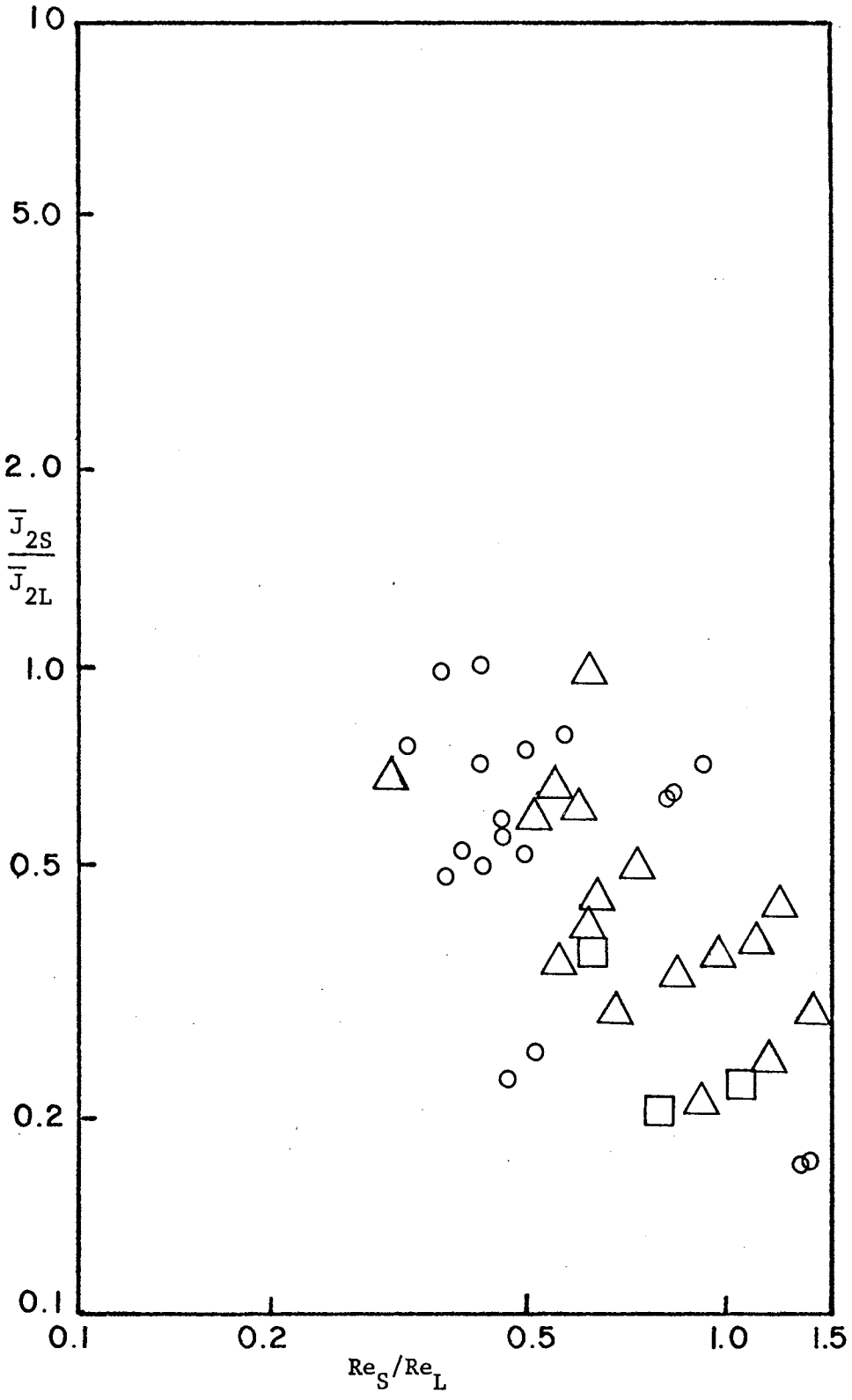

Figure 16. Richardson Parameter Ratio (2) vs. Reynolds Number Ratio. Points are Marked for Top View Similarity

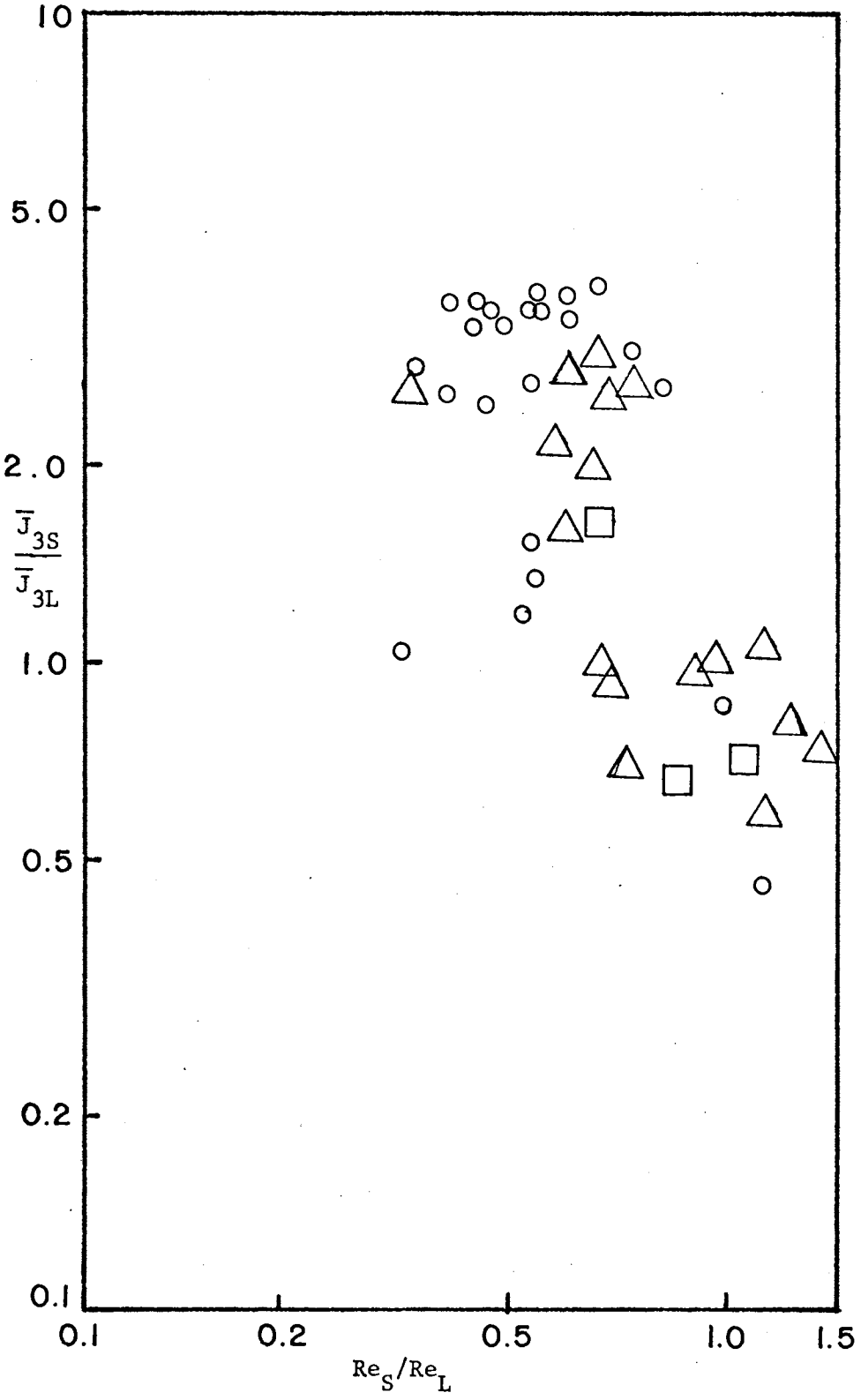

Figure 17. Richardson Parameter Ratio (3) vs. Reynolds Number Ratio. Points are Marked for Top View Similarity

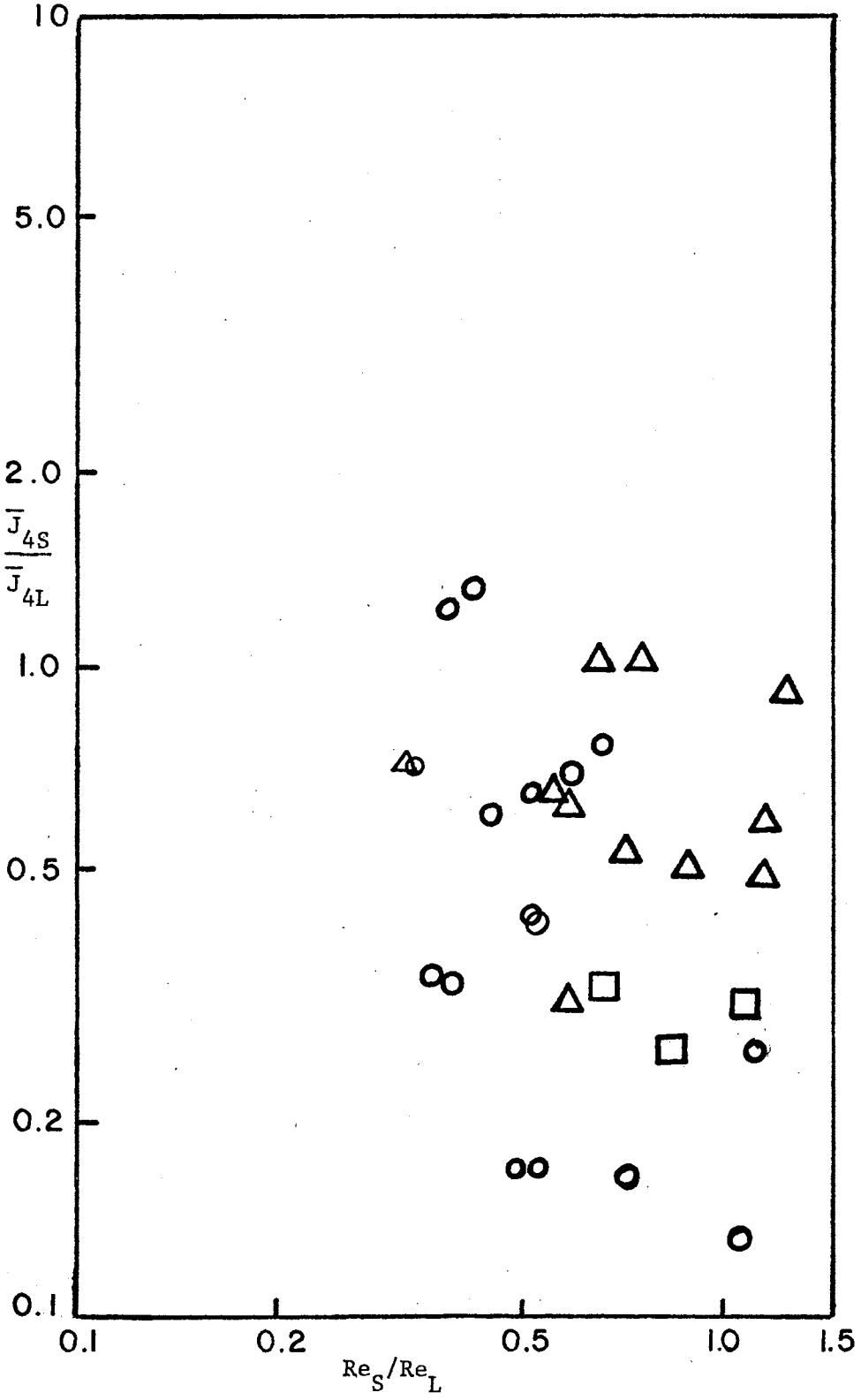

Figure 18. Richardson Parameter Ratio (4) vs. Reynolds Number Ratio. Points are Marked for Top View Similarity

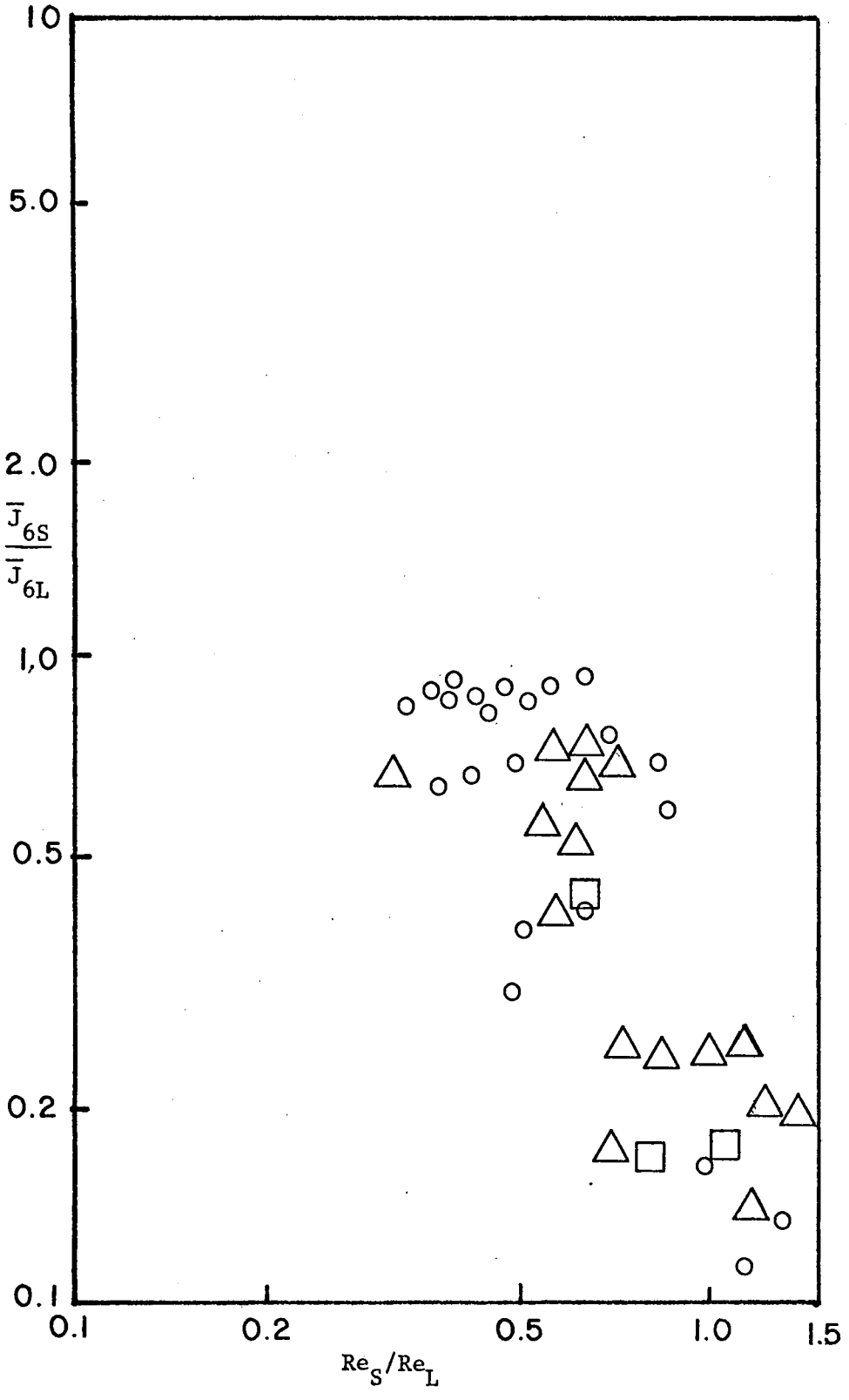

Figure 19. Richardson Parameter Ratio (6) vs. Reynolds Number Ratio. Points are Marked for Top View Similarity

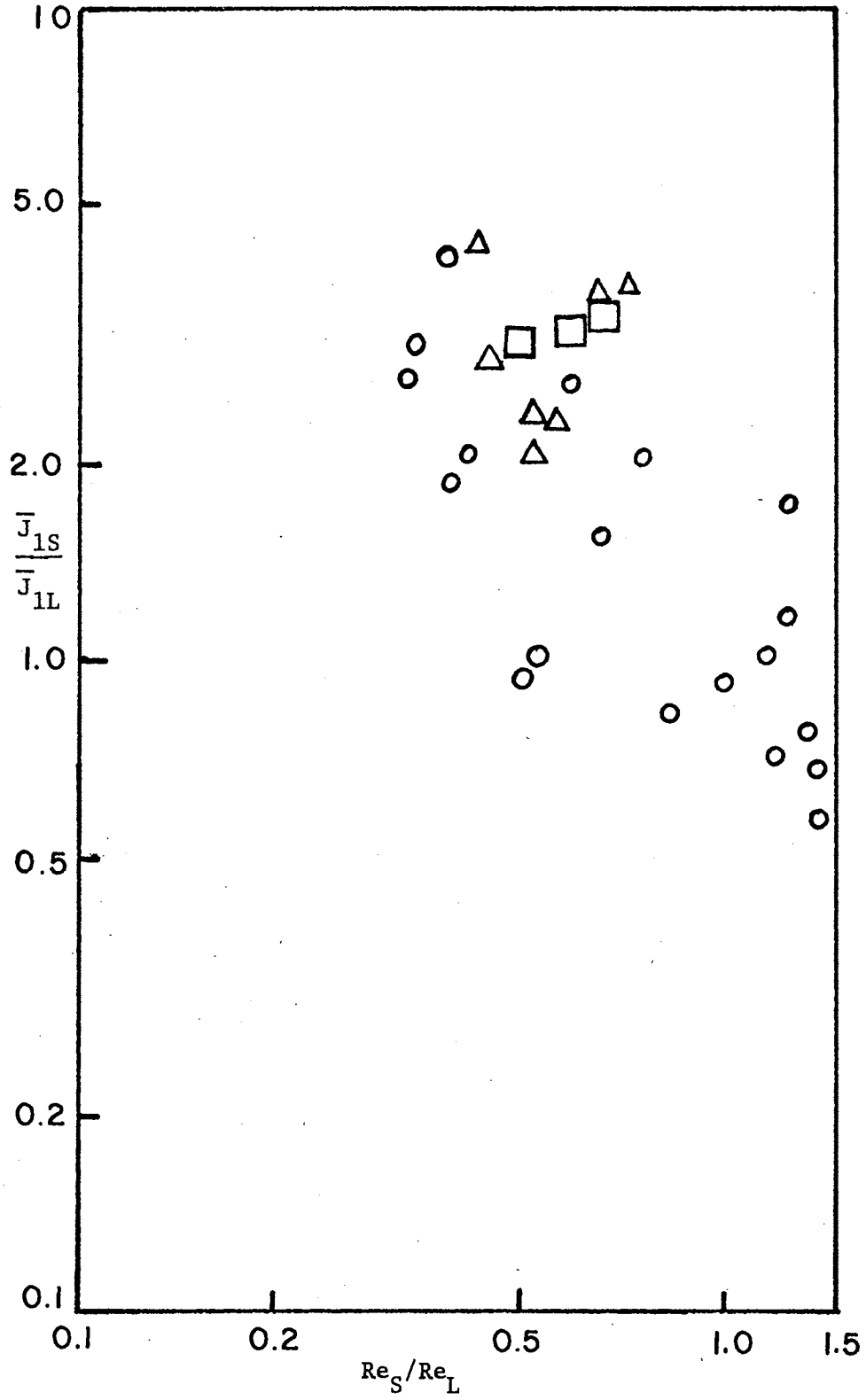

Figure 20. Richardson Parameter Ratio (1) vs. Reynolds Number Ratio. Points are Marked for Side View Similarity

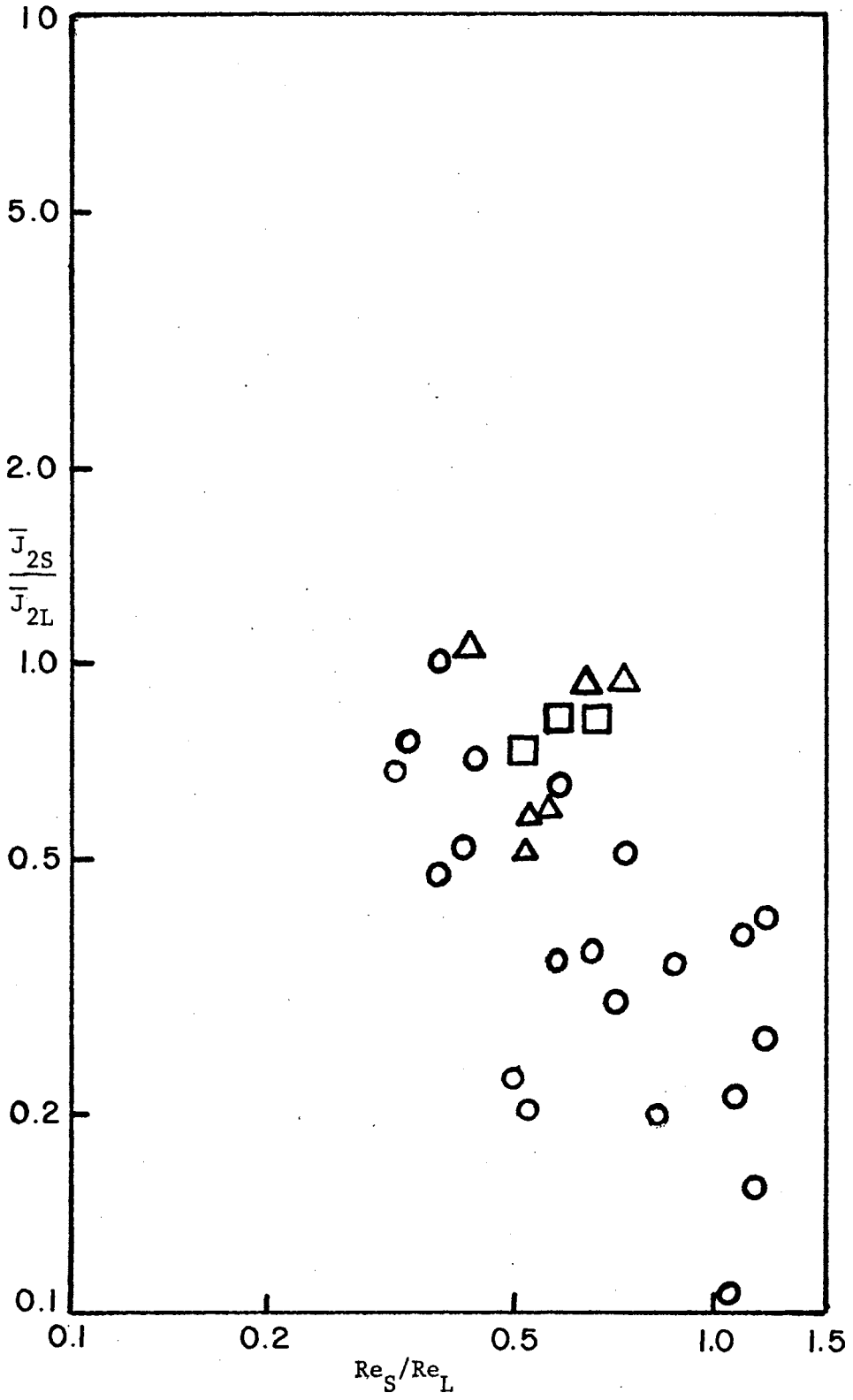

Figure 21. Richardson Parameter Ratio (2) vs. Reynolds Number Ratio. Points are Marked for Side View Similarity

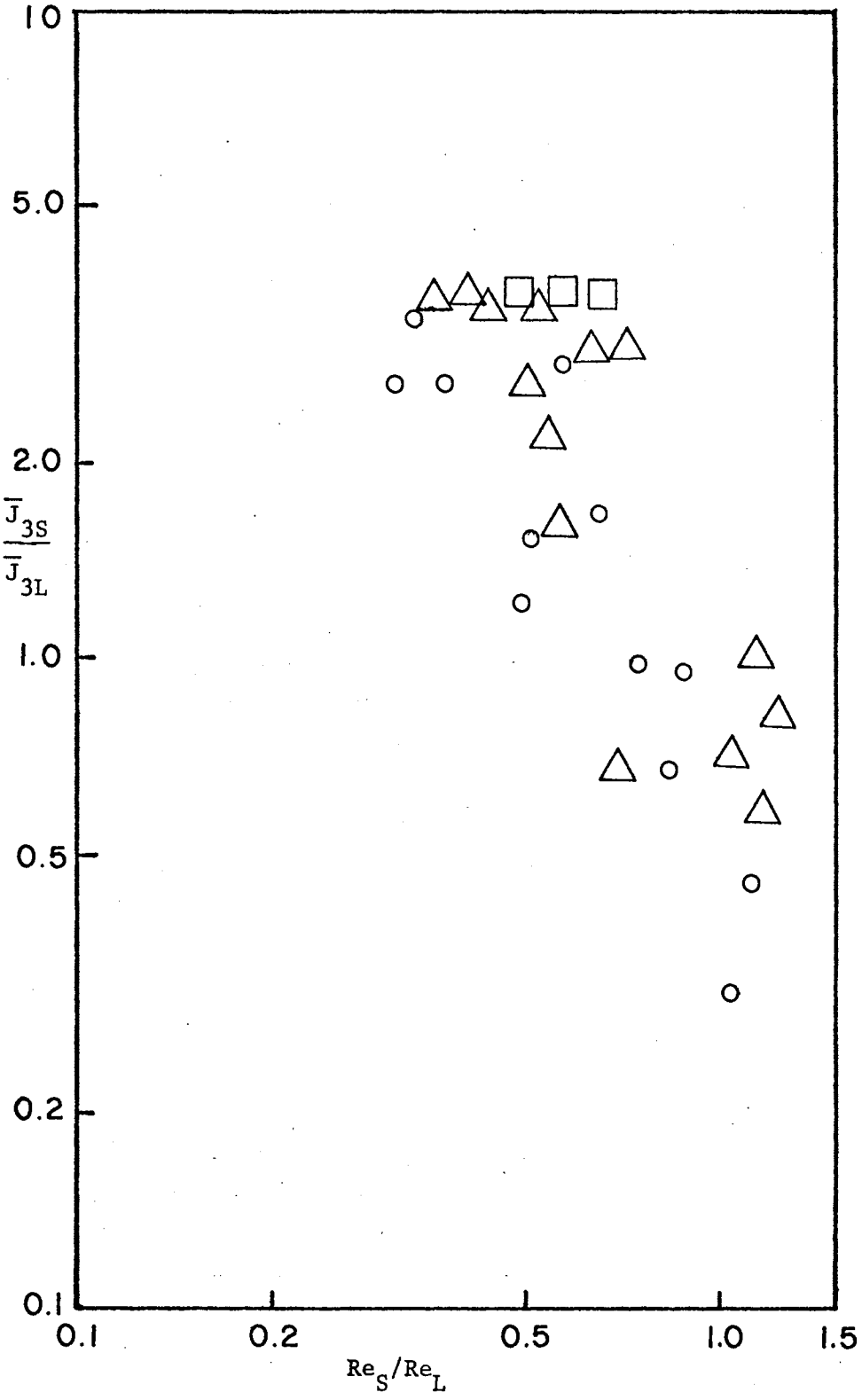

Figure 22. Richardson Parameter Ratio (3) vs. Reynolds Number Ratio. Points are Marked for Side View Similarity

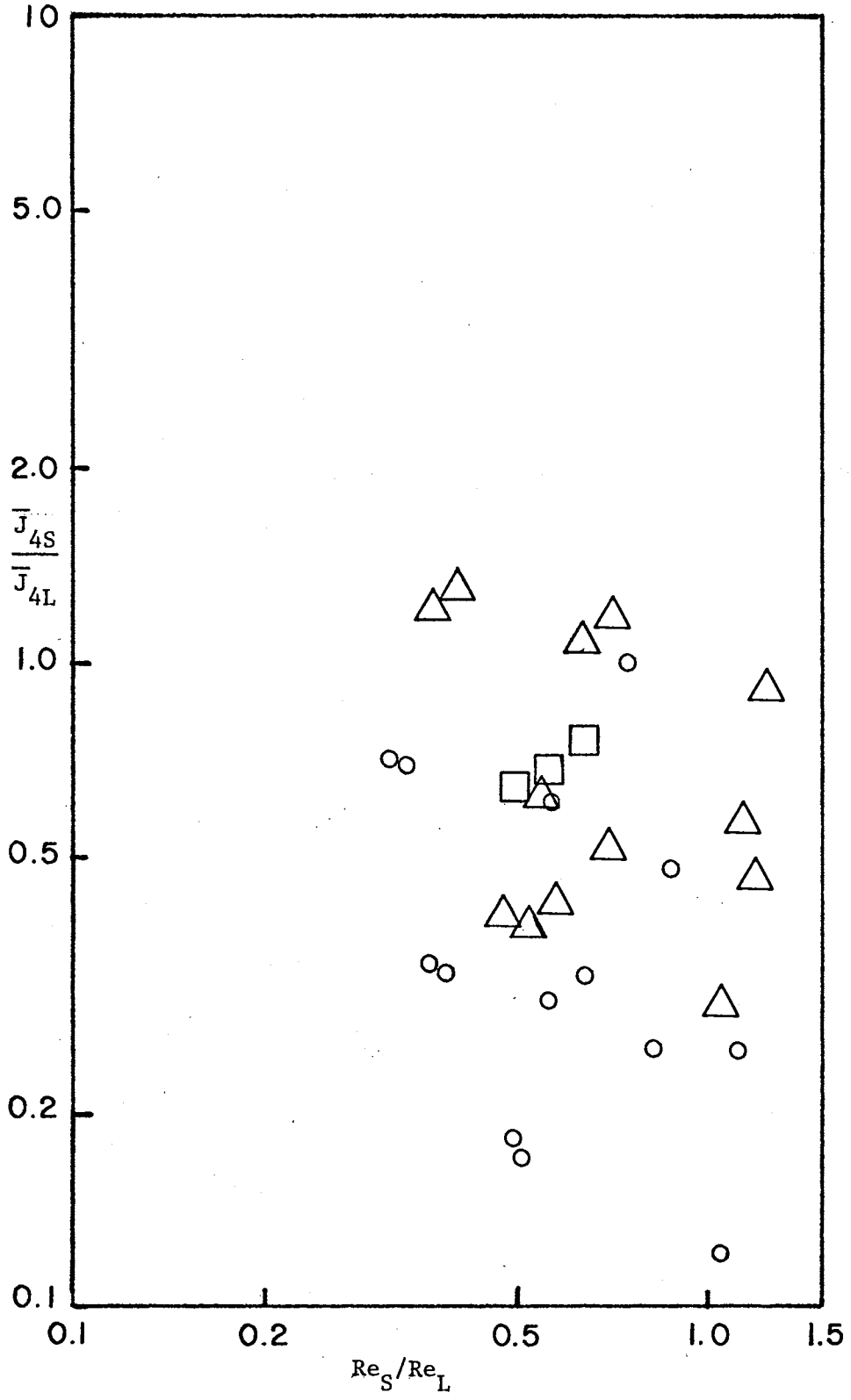

Figure 23. Richardson Parameter Ratio (4) vs. Reynolds Number Ratio. Points are Marked for Side View Similarity

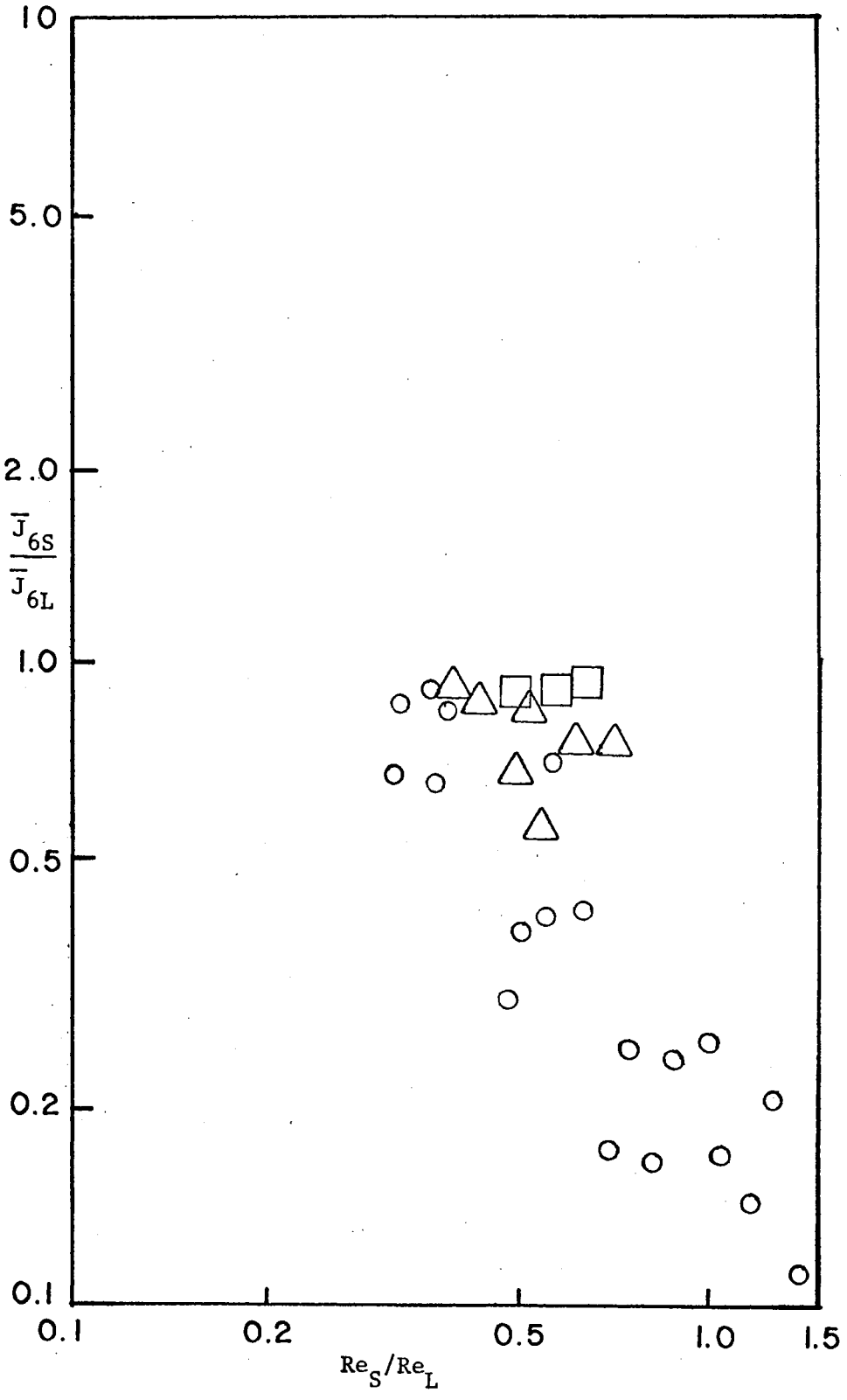

Figure 24. Richardson Parameter Ratio (6) vs. Reynolds Number Ratio. Points are Marked for Side View Similarity

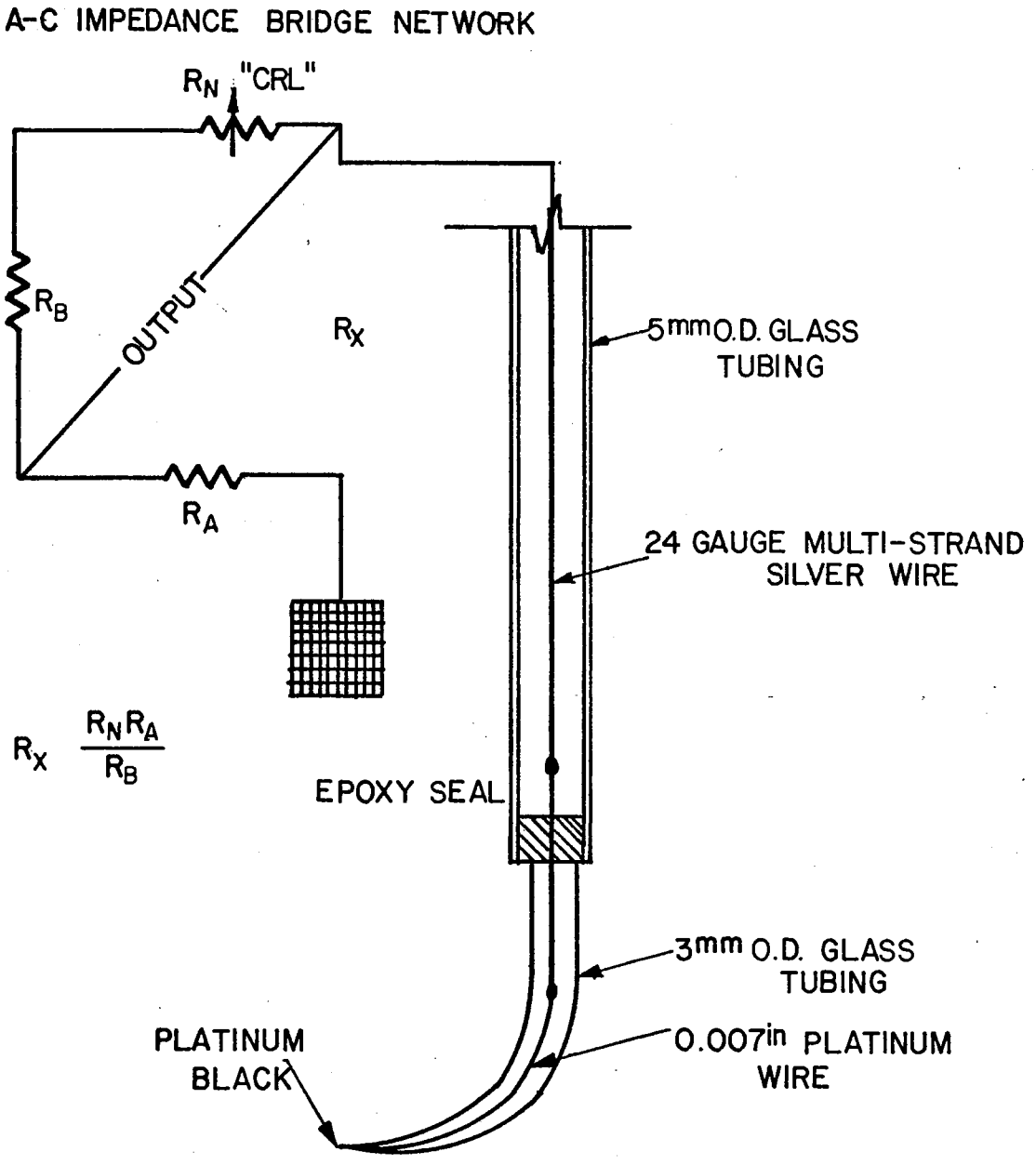

Figure 25. Schematic of Conductivity Probe

TABLE I

MATRIX OF RICHARDSON PARAMETER NUMBERS FOR VARIOUS TEST RUNS

Test No.	J_1	J_2	J_3	J_4	J_5	J_6	Re_D
S-11	327.2	0.1420	735.0	0.3190	0.02813	0.06322	3402
S-14	568.8	0.2469	1197.0	0.5261	0.05573	0.1173	4336
S-15	699.6	0.3036	1554.0	0.6747	0.06150	0.1366	3041
S-16	670.4	0.2910	1578.0	0.6850	0.05250	0.12360	2624
S-17	742.6	0.3224	1650.0	0.7163	0.06528	0.1451	3439
S-19	843.3	0.3662	1349.0	0.5858	0.1431	0.2289	3787
S-20	970.0	0.4212	1617.0	0.7021	0.1516	0.2527	2224
L-10	813.3	1.4119	2324.0	4.0339	0.1730	0.4942	3200
L-11	485.9	0.8436	1620.0	2.8120	0.07593	0.2531	2986
L-12	233.9	0.4061	451.0	0.7830	0.1093	0.2107	6012
L-15	317.5	0.5511	470.3	0.8164	0.2512	0.3721	6642
L-16	224.2	0.3892	448.3	0.7782	0.09733	0.1947	5313
L-17	355.0	0.6162	604.3	1.0489	0.2126	0.3620	6953

VITA

Gene Edward Kouba

Candidate for the Degree of

Master of Science

Thesis: MODELING INFLOWS INTO STRATIFIED LAKES WITH VERTICAL SCALE DISTORTION

Major Field: Mechanical Engineering

Biographical:

Personal Data: Born in El Reno, Oklahoma, February 25, 1949, the son of Mr. and Mrs. Eddie R. Kouba.

Education: Graduated from El Reno High School, El Reno, Oklahoma, in May, 1967; received Bachelor of Science degree in Mechanical Engineering from Oklahoma State University in January, 1972; completed requirements for Master of Science degree at Oklahoma State University in July, 1974.

Professional Experience: Graduate assistant, Oklahoma State University, 1972-73; research assistant, School of Mechanical and Aerospace Engineering, Oklahoma State University, 1973-74.